OUKA
The University of Osaka
Institutional Knowledge Archive

Title	Studies on Bromide Ion Conducting Solids Based on Lanthanum Oxybromide
Author(s)	Misran, Radzi Iqbal Bin Muhammad
Citation	大阪大学, 2021, 博士論文
Version Type	VoR
URL	https://doi.org/10.18910/82214
rights	
Note	

The University of Osaka Institutional Knowledge Archive : OUKA

https://ir.library.osaka-u.ac.jp/

The University of Osaka

Doctoral Dissertation

Studies on Bromide Ion Conducting Solids Based on Lanthanum Oxybromide

(オキシ臭化ランタンを母体とする臭化物イオン伝導体に関する研究)

Muhammad Radzi Iqbal Bin Misran

January 2021

Department of Applied Chemistry
Graduate School of Engineering
Osaka University

Doctoral Dissertation

Studies on Bromide Ion Conducting Solids Based on Lanthanum Oxybromide

(オキシ臭化ランタンを母体とする臭化物イオン伝導体に関する研究)

Muhammad Radzi Iqbal Bin Misran

January 2021

Department of Applied Chemistry
Graduate School of Engineering
Osaka University

Preface

The research for this thesis has been conducted under direct supervision of Professor Dr. Nobuhito Imanaka at the Department of Applied Chemistry, Graduate School of Engineering, Osaka University.

The objective of this thesis is to investigate the bromide ion conduction in lanthanum oxybromide and to reveal the factors affecting the bromide ion conducting properties.

The author hopes that the results and knowledge obtained in this research will contribute to the further design and development of novel solid electrolyte and that the materials would be useful for practical applications in the future.

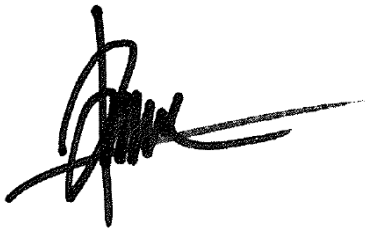

Muhammad Radzi Iqbal Bin Misran

Department of Applied Chemistry

Graduate School of Engineering,

Osaka University,

2-1 Yamadaoka, Suita,

Osaka 565-0871,

JAPAN

January 2021

Contents

General Introduction 1

Chapter 1

The Effects of Bromide Ion Vacancy and Lattice Size on Bromide Ion Conductivity in LaOBr Solids

1.1 Introduction 5

1.2 Experimental Procedure 6

1.3 Results and Discussion 7

1.4 Conclusions 13

Chapter 2

The Control of LaOBr Lattice Size by Divalent Cation Double Doping

2.1 Introduction 14

2.2 Experimental Procedure 15

2.3 Results and Discussion 16

2.4 Conclusions 22

Chapter 3

The Effect of Topical Structural Strain on Bromide Ion Conduction in LaOBr

3.1 Introduction 23

3.2 Experimental Procedure 24

3.3 Results and Discussion 25

3.4 Conclusions 35

Summary 36

References 38

List of Publications 41

Acknowledgements 42

General Introduction

Electrical conduction in solid materials is brought by the migration of charged species such as electron (e^-), hole (h^+), and ion. Among them, the materials whose charge carrier is electronic species (e^- or h^+) are known as metals or semiconductors, and they are widely used as the important parts of devices in various fields. On the other hand, there are unique solids in which the migrant species are ions having non-negligible volume in solid lattice, which is different from electronic species, and they are called “solid electrolytes” or “ion conducting solids”. The distinctive characteristic of solid electrolyte is that the charge carrier is generally limited to only a single ion species because ions in solid are also building components of the lattice, meaning that the solid lattice is destroyed when various kinds of ions conduct simultaneously. Because of such unique characteristic of selective ion migration in a solid material, which is quite different from electrolyte solutions and molten salts, solid electrolyte is expected to be a promising candidate for the key component material for various electrochemical applications such as the all-solid-state batteries, fuel cells and chemical sensors [1-7].

In the field of ion conducting solid, it is widely known that the ionic-size and the valence state of the migrating ion species greatly affect the ion conduction in the solid. The larger the ionic size of the migrating ion species, the more difficult the ion to migrate in the crystal lattice becomes due to the fact that most of the solids have a dense structure without appropriate large space for bulky ions migration. On the other hand, electrostatic interaction between conducting ions and surrounding counter ions become strong with increasing the valence state of conducting species, meaning that the migration of high valent ions in the solid is difficult compared with lower valent ions. Based on this fact, monovalent ions with relatively small ionic-radius such as Li^+ ion (ionic size: 0.090 nm, coordination number (CN) = 6 [8]) [9-11], Na^+ ion (0.116 nm, CN = 6 [8]) [12-14], F^- ion (0.119 nm, CN = 6 [8]) [15-17] etc. are known as the conducting species in the solid, and there are a huge number

of reports on the migration of these ions in solids. Furthermore, divalent ions such as Mg^{2+} ion (0.086 nm, CN = 6 [8]) [18-20], Ca^{2+} ion (0.114 nm, CN = 6 [8]) [21-23], O^{2-} ion (0.126 nm, CN = 6 [8]) [24-26] etc. have been also reported to conduct while the tested temperature were much higher than those for monovalent ions, due to their higher valency than the monovalent ions. In contrast, there are a few reports on the conduction of Cl^- ion (0.165 nm, CN = 6 [8]) or Br^- ion (0.182 nm, CN = 6 [8]) whose ionic size are too large to migrate in rigid crystal lattice while their valence state is −1 as same as the F^- ion. For the Br^- ion conductors, only the $Pb_{0.98}K_{0.02}Br_{1.98}$ [27] and $CsPbBr_3$ [28] solids have been reported until 1995. In addition, these bromide compounds have some critical disadvantages such as low melting point ($PbBr_2$: 373°C [29], $CsPbBr_3$: 510°C [30]) and water-soluble nature ($PbBr_2$: 0.97 g / 100g of water at 25°C [31], $CsPbBr_3$: 123 g / 100g of water at 25°C [32]), which also restricted these bromides to apply for the devices. As a result, the development of the Br^- ion highly conducting solids with high stability is believed to be a hard task in the solid electrolyte fields for long periods.

In order to realize a smooth ion migration in solid lattice, especially for large-size ion, it is essential to select a suitable structure for ion migration such as well-ordered structure, two- or three-dimensional network structure having large open space, and/or the structure with enough defects. Moreover, for obtaining the sufficient chemical and thermal stabilities, it is better to select the compound containing oxygen, in this case, oxybromide, not the simple bromide compound. Because oxide anions form the strong bonding with constituent cations, the oxybromides normally possess higher chemical and thermal stabilities than the corresponding simple bromides.

In the laboratory I belong, rare earth oxybromides, ROBr (R: rare earth) have been paid attention as a candidate for novel bromide ion conducting solid electrolyte. ROBr has the tetragonal matlockite (PbFCl)-type structure with the space group *P*4/*nmm* [33], in which the R^{3+} ion bonds to four O^{2-} anions and four Br^- anions, as shown in **Figure G1**. Moreover, ROBr possesses layered structure consisting the rigid fluorite-type RO layer and the Br layer along *c*-axis. This Br layer is expected to be a conducting pathway for Br^- ion. In addition, since the ROBr has been reported to

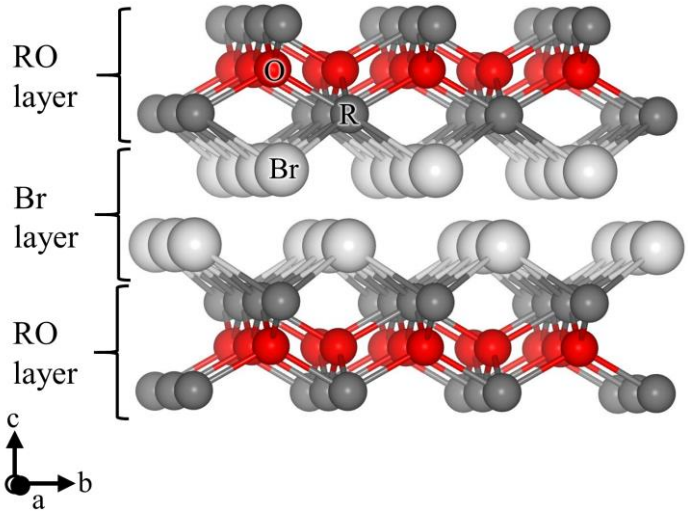

Figure G1. The structure of rare earth oxybromide (ROBr)

show higher thermal stability [34, 35] and water-insoluble nature compared to other bromide compounds [36], rare earth oxybromides are expected to be a good candidate for the mother solid of novel Br^- ion conductor. Among the ROBr, lanthanum oxybromide (LaOBr) possessed the largest lattice volume as well as the highest thermal stability (decomposition temperature: ca. 900°C [35]) and the high water durability (0.056 g / 100 g of water at 25°C [36, 37]). Such a large lattice size of LaOBr realizes large open space in Br layer which is advantageous for the conduction of the Br^- ion. However, the LaOBr itself exhibits low electrical conductivity below 10^{-4} $S \cdot cm^{-1}$ even at 800°C, due to the absence of Br^- ion vacancies which function as the available sites for migration. Therefore, it is essential to introduce the Br^- ion vacancies into the LaOBr structure for obtaining high conductivity. Based on this concept, Imanaka et al. has been successfully improve the Br^- ion conductivity in the LaOBr solid by the substitution of divalent Sr^{2+} ion for the La^{3+} ion site, and it was revealed that the $La_{0.90}Sr_{0.10}OBr_{0.90}$ (the number of Br^- ion vacancies [δ_{Br-}] = 0.10) solid showed ca. 300 times higher conductivity than LaOBr [37].

While the enhancement of Br^- ion conductivity in the LaOBr-type solid was realized by the introduction of Br^- ion vacancies into the LaOBr structure, there remained unclear aspects, those are, what is the origin for exhibiting high Br^- ion conductivity, what is the optimum dopant species and its

amount, and how to improve the Br^- ion conductivity furthermore. In addition, quantitative Br^- ion conduction in the $La_{0.90}Sr_{0.10}OBr_{0.90}$ solid has not been demonstrated yet.

To clarify the above-mentioned points in this thesis, I investigated the effects of lattice volume size and concentration of Br^- ion vacancy on the Br^- ion conduction in the LaOBr solids by the replacement of the La^{3+} site with various kinds of divalent cations.

This thesis consists of the following three chapters.

Chapter 1 deals with the effects of Br^- ion vacancy formation and lattice size on the Br^- ion migration in the LaOBr solid. For this aim, the trivalent La^{3+} ion sites in the LaOBr were partially substituted with alkaline earth metal cations of Mg^{2+}, Ca^{2+}, Sr^{2+}, and Ba^{2+} ion, and the Br^- ion conducting properties in the $La_{0.90}M_{0.10}OBr_{0.90}$ (M = Mg, Ca, Sr, Ba) solids were investigated.

Chapter 2 describes the improvement of Br^- ion migration by increasing the Br^- ion vacancy in the LaOBr-type solid with intentional control of the lattice size of LaOBr by doping two kinds of cation. In order to introduce additional Br^- ion vacancy, the La^{3+} ion sites in the LaOBr were partially replaced by the Sr^{2+} and Ca^{2+} ions simultaneously to inhibit the lattice collapse and the ion conducting properties of the $La_{1-x-y}Sr_yCa_xOBr_{1-x-y}$ solids were investigated.

Chapter 3 discusses the effects of crystal structural strain in the LaOBr on the Br^- ion migration. For discussing this point, Mg^{2+} and Zn^{2+} ions having a similar ionic radius were selected as the co-doping divalent cation of the Sr^{2+} into the La^{3+} ion sites in the LaOBr and investigated the relationship between the structure environment for Br^- ion conduction in the $La_{1-x-y}Sr_yM_xOBr_{1-x-y}$ (M = Mg, Zn) solids. The difference in local structure and Br^- ion conducting nature was explained in terms of the difference of electronegativity of these cations (Mg^{2+} and Zn^{2+}).

Chapter 1

The Effects of Bromide Ion Vacancy and Lattice Size on Bromide Ion Conductivity in LaOBr Solids

1.1. Introduction

In 2003 [37], Imanaka et al. have reported a high Br^- ion conductivity in the $La_{0.90}Sr_{0.10}OBr_{0.90}$ solid of which the trivalent La^{3+} ion site was partially replaced by the divalent Sr^{2+} ion to produce the Br^- ion vacancy in the structure. Although it has been revealed that the generation of Br^- ion vacancy was an important factor for improving the Br^- ion conduction in the LaOBr lattice, there remained experiments which should be carried out for understanding the fundamental knowledge for the ion conducting behavior of the LaOBr-type solid, such as relationship between the lattice size, the amount and the species of dopant, and the Br^- ion conductivity, which are important information for developing a practically applicable Br^- ion conductor in future. Furthermore, the Br^- ion conduction in the $La_{0.90}Sr_{0.10}OBr_{0.90}$ solid has not been quantitatively demonstrated yet.

In this chapter, in order to clarify the effects of not only the formation of Br^- ion vacancy but also the lattice size on the Br^- ion migration in the LaOBr structure, the La^{3+} ion sites in the LaOBr were partially substituted for alkaline earth metal cations of Mg^{2+} (0.103 nm, CN = 8 [8]), Ca^{2+} (0.126 nm, CN = 8 [8]), Sr^{2+} (0.140 nm, CN = 8 [8]), or Ba^{2+} (0.156 nm, CN = 8 [8]) ion, and the Br^- ion conducting properties in the $La_{0.90}M_{0.10}OBr_{0.90}$ (M = Mg, Ca, Sr, Ba) solids were investigated. Here, we held the doping amount of M to be 0.10 in order to compare the results to the previously reported $La_{0.90}Sr_{0.10}OBr_{0.90}$ solid. In addition, the Br^- ion migration in the $La_{0.90}Sr_{0.10}OBr_{0.90}$ solid was also directly determined by modified Tubandt electrolysis method.

1.2. Experimental Procedure

Alkaline metal cation doped lanthanum oxybromide, $La_{0.90}M_{0.10}OBr_{0.90}$ (M = Mg, Ca, Sr, Ba) solids, were synthesized by solid-state reaction method. Powders of La_2O_3, $M(NO_3)_2 \cdot xH_2O$ (M = Mg (x = 6), Ca (x = 4), Sr (x = 0), Ba (x = 0)), and NH_4Br were mixed at a La : M : Br ratio of 0.90 : 0.10 : 1.80 using an agate mortar, and then calcined at 800°C for 12 h under synthetic air flow.

The phase of the samples was identified by X-ray powder diffraction (XRD; SmartLab, Rigaku) performed with Cu-Kα radiation (40 kV, 30 mA). XRD data were collected in the 2θ range of 10 to 70° at a scan speed of 8 degree·min^{-1} and a step width of 0.04°. The lattice volume of the LaOBr-type phase was estimated from the XRD profile obtained by using α-Al_2O_3 as a standard material.

For the electrical conductivity measurements, the sample powder was pressed into a pellet and sintered at 800°C for 12 h under synthetic air flow. Thereafter, the pellet was polished with waterproof abrasive papers (#1000, 2000, 3000, and then 8000), and the platinum-sputtered layers were formed on the polished center surfaces of the pellet using an ion coater (IB-3, Eiko). After then, the platinum paste was additionally fixed on the sputtered layer for the conductivity measurements at temperature above 600°C. Ac conductivity (σ_{ac}) measurement of the sample pellet was conducted by a complex impedance method in the frequency range of 5 Hz to 13 MHz (1260 Impedance/Gain-Phase Analyzer, Solartron) at the temperature range of 800 to 300°C in the atmospheric air.

To identify the conducting species in the $La_{0.90}Sr_{0.10}OBr_{0.90}$ solid, modified Tubandt electrolysis was performed by applying a dc voltage of 1.0 V to three pellets (one La_2O_3 pellet and two $La_{0.90}Sr_{0.10}OBr_{0.90}$ pellets were attached from the anodic to cathodic direction) sandwiched by the platinum electrodes at 800°C for 24 h in the atmospheric air. For each pellet, the weights before and after the electrolysis were measured. In addition, the elemental distribution in the electrolyzed pellets was examined by cross-sectional line analysis by means of a scanning electron microscope (SEM) equipped with an energy dispersive X-ray (EDX) analyzer (SSX-550, Shimadzu).

1.3. Results and Discussion

Figure 1.1 shows the XRD patterns of the $La_{0.90}M_{0.10}OBr_{0.90}$ (M = Mg, Ca, Sr, Ba) solids with the mother LaOBr. The samples doped with Mg, Ca, or Sr were a single-phase solid with the LaOBr-type structure, whereas the sample with M = Ba was obtained as a mixture of LaOBr-type solid, La_2O_3 and BaO. **Figure 1.2** displays the lattice volume of the LaOBr-phase in the obtained samples with the corresponding value of the LaOBr solid, which was calculated from the XRD peak angles. For the single-phase samples with M = Mg, Ca, Sr, the lattice volume increased with increasing the ionic radius of the dopant cation (Mg^{2+} (0.103 nm, CN = 8 [8]), Ca^{2+} (0.126 nm, CN = 8 [8]), Sr^{2+} (0.140 nm, CN = 8 [8])). Furthermore, the lattice volumes for the $La_{0.90}M_{0.10}OBr_{0.90}$ (M = Mg, Ca) solids were smaller than that of LaOBr, and the $La_{0.90}Sr_{0.10}OBr_{0.90}$ solid has larger lattice volume compared with LaOBr, which is reasonable tendency speculated from the difference of ionic radius of cations ($Mg^{2+} < Ca^{2+} <$

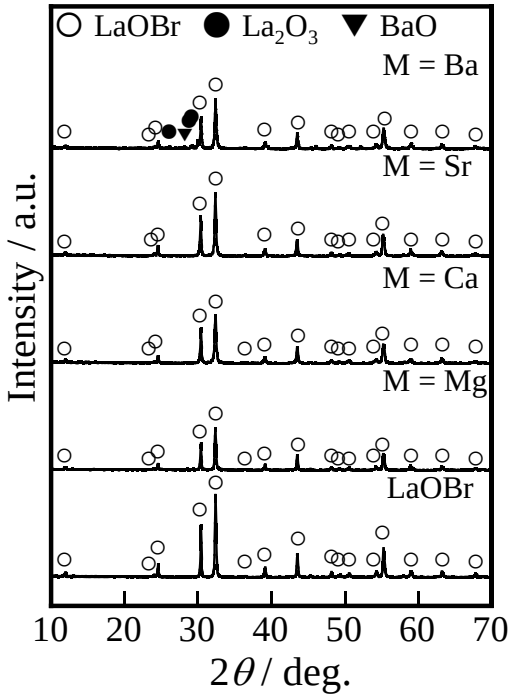

Figure 1.1. XRD patterns of the $La_{0.90}M_{0.10}OBr_{0.90}$ (M = Mg, Ca, Sr, Ba) solids.

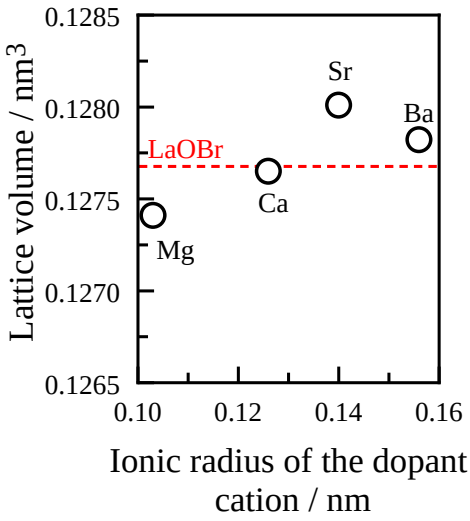

Figure 1.2. The lattice volume of the $La_{0.90}M_{0.10}OBr_{0.90}$ (M = Mg, Ca, Sr, Ba) solids. Red dashed line indicates the lattice volume of mother LaOBr.

La^{3+}(0.130 nm, CN = 8 [8]) < Sr^{2+}). From these results, it was confirmed that these dopant cations (Mg^{2+}, Ca^{2+}, Sr^{2+}) were successfully partially substituted for the La^{3+} ion in the solids. On the other hand, for the $La_{0.90}Ba_{0.10}OBr_{0.90}$ solid, although the lattice expansion compared to the LaOBr solid was observed by doping large Ba^{2+} ion (0.156 nm, CN = 8 [8]), the lattice volume of the LaOBr-phase formed in the $La_{0.90}Ba_{0.10}OBr_{0.90}$ solid (mixed-phase solid) was smaller than that of the $La_{0.90}Sr_{0.10}OBr_{0.90}$ solid (single-phase solid). From this result, it was speculated that only a few amounts of Ba^{2+} ion (less than 0.10) were doped into the La^{3+} ion site.

Figure 1.3 displays the temperature dependence of the Br^- ion conductivity in the $La_{0.90}M_{0.10}OBr_{0.90}$ (M = Mg, Ca, Sr, Ba) solids, with the corresponding data for the mother LaOBr solid. The conductivities of all samples were higher than that of LaOBr, due to the formation of Br^- ion vacancy by introducing the lower valent cations into the La^{3+} ion site. In addition, for the single-phase samples, the conductivity was increased in the order of $La_{0.90}Mg_{0.10}OBr_{0.90}$ < $La_{0.90}Ca_{0.10}OBr_{0.90}$ < $La_{0.90}Sr_{0.10}OBr_{0.90}$. Furthermore, the activation energy for Br^- ion migration in solid (The Br^- ion migration is demonstrated below in this chapter.), on the contrary, was decreased in the order of $La_{0.90}Mg_{0.10}OBr_{0.90}$ (93.5 $kJ \cdot mol^{-1}$) > $La_{0.90}Ca_{0.10}OBr_{0.90}$ (92.8 $kJ \cdot mol^{-1}$) > $La_{0.90}Sr_{0.10}OBr_{0.90}$ (84.3

kJ·mol^{-1}). Since these tendencies were well coincided with the order of lattice volume of the $La_{0.90}M_{0.10}OBr_{0.90}$ (M = Mg, Ca, Sr) solid (see, **Figure 1.2**), it is assumed that the Br^- ion conductivity in the $La_{0.90}M_{0.10}OBr_{0.90}$ (M = Mg, Ca, Sr) solids was strongly affected by the lattice volume, and smooth Br^- ion migration was expected to obtain for the expanded lattice of LaOBr. On the other hand, the conductivity of $La_{0.90}Ba_{0.10}OBr_{0.90}$ was placed between those of the solids with M = Sr, Ca, which is easily speculated from the lattice volume, the activation energy for the $La_{0.90}Ba_{0.10}OBr_{0.90}$, (98.7 kJ·mol^{-1}) was higher to that of the solid with M = Mg. Such high activation energy beyond the speculation of the order of lattice volume was attributed by the formation of impurity phase.

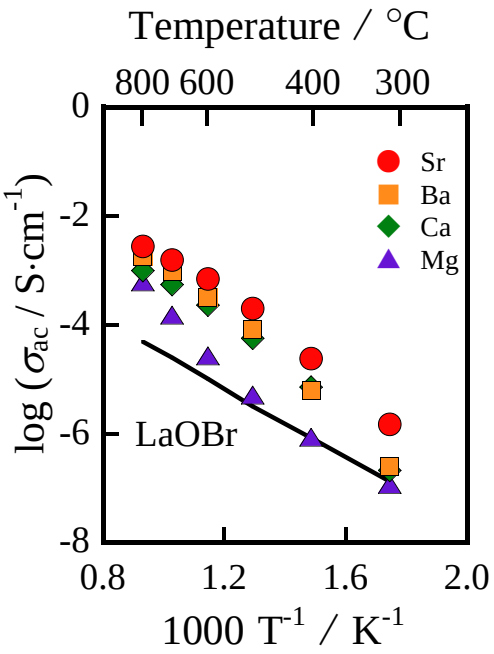

Figure 1.3. Temperature dependencies of the ac conductivity for the $La_{0.90}M_{0.10}OBr_{0.90}$ (M = Mg, Ca, Sr, Ba) and LaOBr (—) solids.

As mentioned in the introduction of this chapter, quantitative demonstration of Br^- ion conduction in the $La_{0.90}Sr_{0.10}OBr_{0.90}$ solid has not been carried out while a qualitative one was accomplished in 2003 [37]. Therefore, a modified Tubandt electrolysis was conducted by applying the

dc voltage of 1.0 V (decomposition voltage of the $La_{0.90}Sr_{0.10}OBr_{0.90}$ solid: ca. 0.9 V). Here, for the quantitative demonstration of Br^- ion migration, I applied one La_2O_3 sample (pellet A) and two $La_{0.90}Sr_{0.10}OBr_{0.90}$ samples (pellet B and C), which were set up with platinum blocking electrodes positioned at both anodic and cathodic side of the cell as shown in **Figure 1.4**. Mechanism for demonstration of Br^- ion migration by this method is as follows. By applying enough dc voltage for the generation of Br^- ions inside the $La_{0.90}Sr_{0.10}OBr_{0.90}$ pellet with the sample decomposition, the Br^- ions should be generated in the cathodic $La_{0.90}Sr_{0.10}OBr_{0.90}$ pellet (pellet C):

$$\frac{10}{9}La_{0.90}Sr_{0.10}OBr_{0.90} + \frac{1}{4}O_2 + e^- \rightarrow \frac{1}{2}La_2O_3 + \frac{1}{9}SrO + Br^- \qquad (1)$$

The Br^- ions generated in the pellet C conduct through middle part of $La_{0.90}Sr_{0.10}OBr_{0.90}$ pellet (pellet B), and then reach to La_2O_3 (pellet A). At the surface of La_2O_3 (pellet A) contacted with $La_{0.90}Sr_{0.10}OBr_{0.90}$ pellet (pellet B), the Br^- ions reached should react with La_2O_3 to produce LaOBr:

$$\frac{1}{2}La_2O_3 + Br^- \rightarrow LaOBr + \frac{1}{4}O_2 + e^- \qquad (2)$$

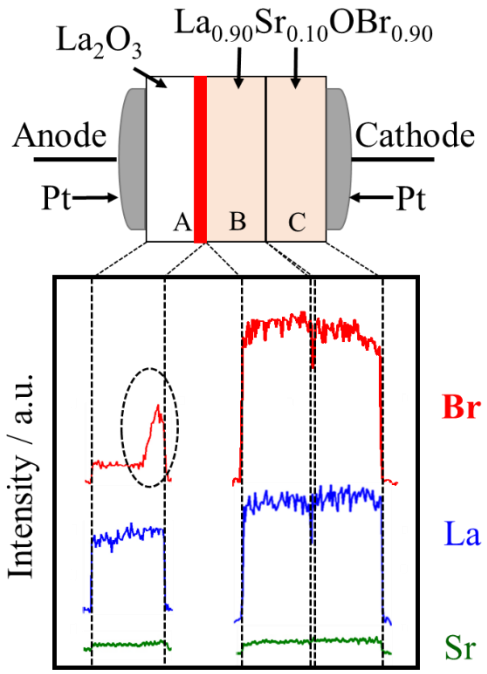

Figure 1.4. Modified Tubandt electrolysis cell set up using La_2O_3 and $La_{0.90}Sr_{0.10}OBr_{0.90}$ pellets and the results of EDX line analysis after the electrolysis applied at 1.0 V, 800°C for 24 h in air.

Figure 1.4 also shows the cross-sectional elemental distribution inside the three pellets after the electrolysis measured by the line analysis using energy dispersive X-ray analyzer (EDX). Only segregation of Br was clearly observed inside but near the cathodic surface of the La_2O_3 pellet (A) in contact with $La_{0.90}Sr_{0.10}OBr_{0.90}$ pellet (B). Furthermore, since the Br concentration in the cathodic pellet C gradually decreased from anodic to cathodic direction, it is suggested that Br^- ion migrated from the cathodic $La_{0.90}Sr_{0.10}OBr_{0.90}$ pellet to the anodic La_2O_3 pellet. Moreover, the weight changes of the electrolyzed pellets were also examined to quantitatively demonstrate the Br^- ion conduction. The theoretical weight changes were calculated from the total electric charge passed during the electrolysis, and the weight change caused by the thermal decomposition of the sample was compensated by weighing the reference pellets of La_2O_3 and $La_{0.90}Sr_{0.10}OBr_{0.90}$ which were not applied to a dc voltage, similar to previous paper [38]. If Br^- ion is the migrating species, the weight gain of the pellet A and the corresponding weight loss of the pellet C should be observed, whereas no weight change is observed in the middle pellet B because Br^- ion only migrates through the pellet B. **Table 1.1** lists the observed weight changes of each pellet during the electrolysis, with the theoretical values in the case of Br^- ion migration. A weight increase of La_2O_3 at the anodic side (pellet A) and a weight decrease of cathodic side (Sum of weight for pellets B and C was measured due to adhesion of these pellets.) were obviously confirmed, whose change were in good accordance with the theoretical ones of Br^- ion conduction; i.e., the measured / theoretical weight change ratios were ca. 95%. This result strongly indicates that the Br^- ion is the migrating species in the $La_{0.90}Sr_{0.10}OBr_{0.90}$ solid.

Table 1.1. Theoretical and observed weight changes for the electrolyzed La_2O_3 (pellet A) and $La_{0.90}Sr_{0.10}OBr_{0.90}$ (pellets B and C)

Pellet	Theoretical weight change / mg	Observed weight change / mg	Observed / theoretical weight change
A	+0.273	+0.258	94 %
B	0	−0.260	95 %
C	−0.273		

Although the weight change reached to 95 % of theoretical one was observed by the modified Tubandt electrolysis, there remains a possibility of O^{2-} ion and electron conduction in the solid. To eliminate the probability of O^{2-} ion and electron migration in $La_{0.90}Sr_{0.10}OBr_{0.90}$, polarization behavior was also examined by investigating the change of dc to ac conductivity ratio (σ_{dc}/σ_{ac}) with time in high and low oxygen partial pressure atmospheres. The dc conductivity performed by applying a lower dc voltage than the decomposition one provides information about the migrating species [39]. For the O^{2-} ion conductor, the dc conductivity should be nearly equal to the ac conductivity under the O_2 atmosphere where the conducting species (O^{2-} ion) can be supplied continuously from the atmospheric O_2. However, under the low oxygen partial pressure atmosphere such as Ar atmosphere, the dc conductivity drastically lowered with time because O^{2-} ions cannot be supplied from the atmosphere. In the case of electronic conductors, dc conductivity should be similar to the ac conductivity regardless of the atmosphere because the migrating electrons can be supplied from the electrode, meaning that the σ_{dc}/σ_{ac} value would be ca. 1. However, for the cation or bromide ion conducting solids, the conducting species cannot be supplied from not only atmosphere but also electrodes. Therefore, the σ_{dc}/σ_{ac} value reduces drastically over time in any atmosphere. **Figure 1.5** depicts the time dependencies of the σ_{dc}/σ_{ac} ratio at 800°C in O_2 and Ar atmospheres. In both atmospheres, the ratio

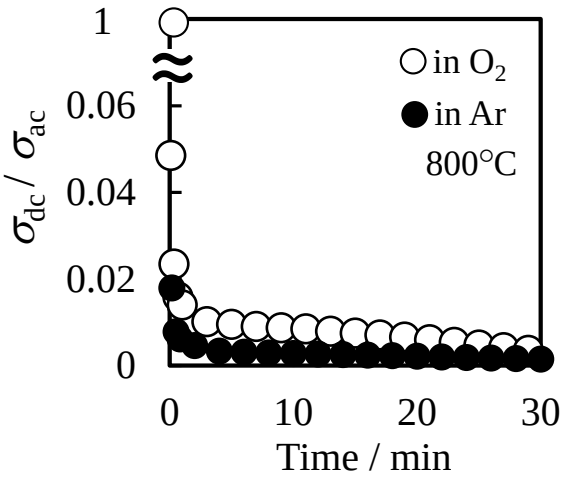

Figure 1.5. σ_{dc}/σ_{ac} ratio for the $La_{0.90}Sr_{0.10}OBr_{0.90}$ solid in O_2 and Ar as a function of time.

drastically decreased and reached to less than 0.02 after 30 minutes, indicating that oxide ion and electron were eliminated from the candidate for the major conducting species in the $La_{0.90}Sr_{0.10}OBr_{0.90}$ solid. From this result, it was concluded that the 5% error in weight change observed for the modified Tubandt electrolysis was caused by the leak current flowed outside the sample pellet during the experiment and that the Br^- ion migration in $La_{0.90}Sr_{0.10}OBr_{0.90}$ solid was quantitatively demonstrated.

1.4. Conclusions

In order to reveal the effects of bromide ion vacancy and lattice size on bromide ion conduction in the LaOBr solid, the conducting properties of the $La_{0.90}M_{0.10}OBr_{0.90}$ (M = Mg, Ca, Sr, Ba) solids were investigated in detail. The formation of Br^- ion vacancy greatly improved the electrical conductivity of LaOBr solid, and the Br^- ion conductivity was enhanced by the expansion of lattice volume. Among the samples prepared, the $La_{0.90}Sr_{0.10}OBr_{0.90}$ solid having the largest lattice volume in the single-phase samples showed the highest Br^- ion conductivity. Therefore, it was clear that the enhancement of the Br^- ion conductivity is achieved by the introduction of Br^- ion vacancy and the enlargement of Br^- ion conducting pathway. The Br^- ion conduction in the $La_{0.90}Sr_{0.10}OBr_{0.90}$ solid was quantitatively demonstrated by means of modified Tubandt electrolysis method combining the La_2O_3 and $La_{0.90}Sr_{0.10}OBr_{0.90}$ solids.

Chapter 2

The Control of LaOBr Lattice Size by Divalent Cation Double Doping

2.1. Introduction

In Chapter 1, the improvement of the conductivity has been succeeded by partially substituting the La^{3+} ion site in LaOBr with divalent cation to introduce Br^- ion vacancies as a result of charge compensation, and it was revealed that the $La_{0.90}Sr_{0.10}OBr_{0.90}$ solid having the largest lattice volume among the $La_{0.90}M_{0.10}OBr_{0.90}$ (M = Mg, Ca, Sr, Ba) solids prepared showed ca. 300 times higher conductivity than that of LaOBr. This result suggested a possibility for further improvement of Br^- ion conductivity by the additional doping of Sr^{2+} into the La^{3+} site to generate higher concentration of Br^- ion vacancy. However, excessive introduction of large-sized Sr^{2+} ions (0.140 nm, CN = 8 [8]) into La^{3+} ion (0.130 nm, CN = 8 [8]) site causes the decomposition of $La_{1-x}Sr_xOBr_{1-x}$ solid to LaOBr-type solid, La_2O_3 and $SrBr_2$ due to the lattice collapse originated by large ionic size of Sr^{2+}. Therefore, the strict control of the lattice size is essential to produce further amount of Br^- ion vacancy in the $La_{1-x}Sr_xOBr_{1-x}$ solid.

In this chapter, I additionally substituted the La^{3+} ion (0.130 nm, CN = 8 [8]) site in the $La_{1-x}Sr_xOBr_{1-x}$ solid with the smaller ionic size of Ca^{2+} ion (0.126 nm, CN = 8 [8]) to introduce further Br^- ion vacancies with inhibiting the lattice expansion, and the Br^- ion conducting properties of the $La_{1-x-y}Sr_xCa_yOBr_{1-x-y}$ solids were investigated.

2.2. Experimental Procedure

$La_{1-x-y}Sr_xCa_yOBr_{1-x-y}$ solids were synthesized by solid-state reaction. Stoichiometric amount of La_2O_3, $Sr(NO_3)_2$, $Ca(NO_3)_2 \cdot 4H_2O$, and NH_4Br were mixed using an agate mortar and the mixed powder was preheated at 800°C for 12 h in synthetic air flow. The obtained powder was pressed into a pellet and calcined at 800°C for 12 h several times to obtain the single-phase sample.

The samples prepared were identified by X-ray powder diffraction (XRD; SmartLab, Rigaku) performed with Cu-Kα radiation (40 kV, 30 mA). XRD patterns were collected in the 2θ range between 10 and 70 degree at a scan speed of 8 degree·min^{-1} and a step scan width of 0.04 degree. The lattice volume of the sample was estimated by refining the XRD peak angles using α-Al_2O_3 as a standard material.

For the electrical conductivity measurements, the sample powder was pressed into a pellet and sintered at 800°C for 12 h in synthetic air flow. Thereafter, the sintered pellet was polished with the waterproof abrasive papers, the platinum sputtered layers were formed on center surfaces of the pellet by using ion coater (IB-3, Eiko), followed by applying platinum paste on the sputtered layer. The ac conductivity (σ_{ac}) measurement of the sample pellet was conducted by a complex impedance method in the frequency range from 5 Hz to 13 MHz (1260 Impedance/Gain-Phase Analyzer, Solartron) at cooling step from 800 to 300°C in atmospheric air.

Similar to the case for the $La_{0.90}Sr_{0.10}OBr_{0.90}$ solid (Chapter 1), modified Tubandt electrolysis was carried out for the $La_{0.85}Sr_{0.10}Ca_{0.05}OBr_{0.85}$ sintered pellet by applying a dc voltage of 0.7 V at 700°C for 4 h in the atmospheric air. The weight change and the elemental distribution in the electrolyzed pellets were confirmed with similar manner described in Chapter 1.

2.3. Results and Discussion

In order to optimize the composition of the $La_{1-x-y}Sr_xCa_yOBr_{1-x-y}$ solid exhibiting the highest conductivity, two-step optimization was carried out; i.e., after identifying the optimal Ca composition (y) by fixing the Sr content (x) at 0.10, the Sr amount was optimized. **Figure 2.1** shows the XRD patterns of the $La_{0.90-y}Sr_{0.10}Ca_yOBr_{0.90-y}$ solids ($0 \le y \le 0.15$). The samples with $y \le 0.05$ were obtained as a single-phase solid with LaOBr-type structure, whereas the samples with $y > 0.05$ were two-phase mixture of the LaOBr-type solid and $SrBr_2$. This result indicates that the solid solubility limit of Ca (y) for the $La_{0.90-y}Sr_{0.10}Ca_yOBr_{0.90-y}$ solids is $y = 0.05$. **Figure 2.2** depicts the lattice volume for the $La_{0.90-y}Sr_{0.10}Ca_yOBr_{0.90-y}$ solids as a function of the Ca^{2+} ion content (y). For the single-phase samples with $y \le 0.05$, the lattice volume of the LaOBr-type phase decreased with increasing Ca^{2+} ion content, suggesting that the smaller Ca^{2+} ion (0.126 nm, CN = 8 [8]) was substituted for the La^{3+} ion (0.130 nm, CN = 8 [8]) site, which is a reasonable tendency observed for the substitutional-type solid

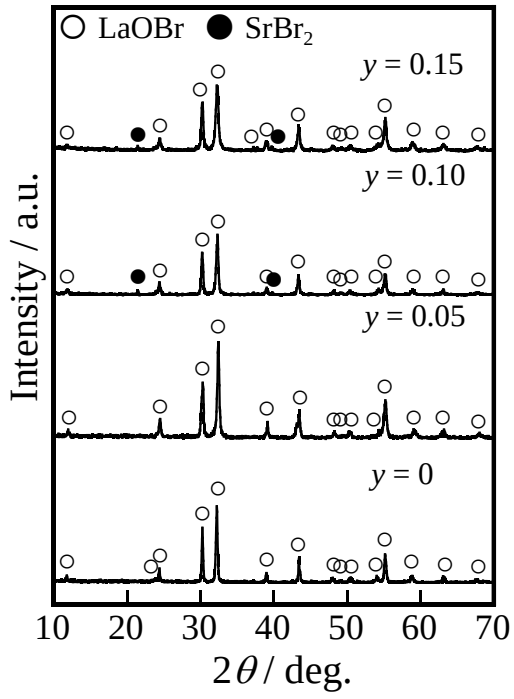

Figure 2.1. XRD patterns of the $La_{0.90-y}Sr_{0.10}Ca_yOBr_{0.90-y}$ ($0 \le y \le 0.15$) solids.

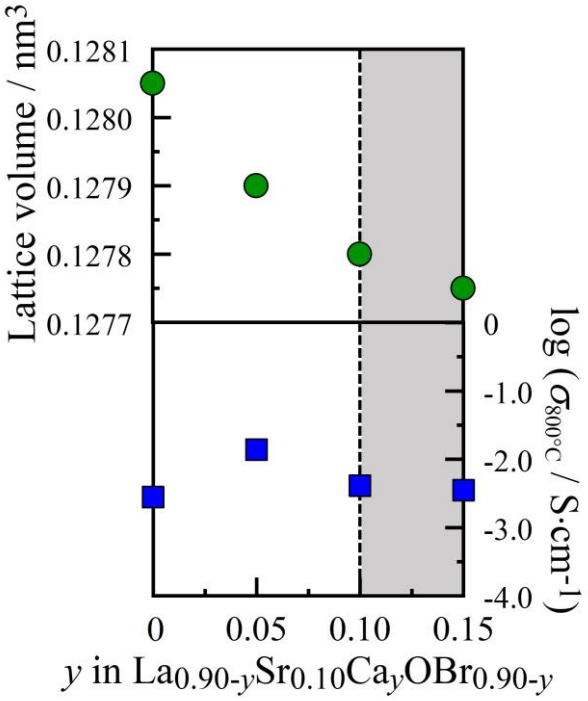

Figure 2.2. Lattice volume and conductivity at 800°C for the $La_{0.90-y}Sr_{0.10}Ca_yOBr_{0.90-y}$ solids as a function of the Ca^{2+} ion content (y).

solution. However, further decrease of the lattice volume was observed even in the two-phase mixture region ($y > 0.05$). This unexpected tendency from the substitutional-type solid solution gives us an assumption that the preferential substitution of the smaller Ca^{2+} ion than Sr^{2+} into the La^{3+} ion site was occurred. As a result, Sr^{2+} amount doped into the La^{3+} site was reduced compared with the solid with $y = 0.05$, and excess amount of Sr^{2+} which cannot replace the La^{3+} site might precipitated as $SrBr_2$; which is supported by **Figure 2.1**. **Figure 2.2** also depicts the ac conductivity at 800°C for the $La_{0.90-y}Sr_{0.10}Ca_yOBr_{0.90-y}$ solids as a function of Ca^{2+} ion content (y). In the single-phase region, the conductivity increased with increasing Ca^{2+} content (y), and the highest conductivity was obtained for the solid solubility limit composition, $La_{0.85}Sr_{0.10}Ca_{0.05}OBr_{0.85}$ ($y = 0.05$), due to the increase of Br^- ion vacancies. However, in the two-phase mixture region of $y > 0.05$, the conductivity decreased by both the shrinkage of the lattice and the appearance of impurity phase.

Since the optimum Ca content in the $La_{0.90-y}Sr_{0.10}Ca_yOBr_{0.90-y}$ solid was revealed to be $y =$

0.05, the Sr^{2+} ion doping amount (x) of the La^{3+} ion site was optimized for the $La_{0.95-x}Sr_xCa_{0.05}OBr_{0.95-x}$ solids. **Figure 2.3** displays the XRD patterns of the $La_{0.95-x}Sr_xCa_{0.05}OBr_{0.95-x}$ ($0 \leq x \leq 0.15$) solids. The samples with $x \leq 0.10$ possessed a single-phase of LaOBr-type structure, whereas the sample with x = 0.15 was a mixture of the LaOBr-type solid and $SrBr_2$.

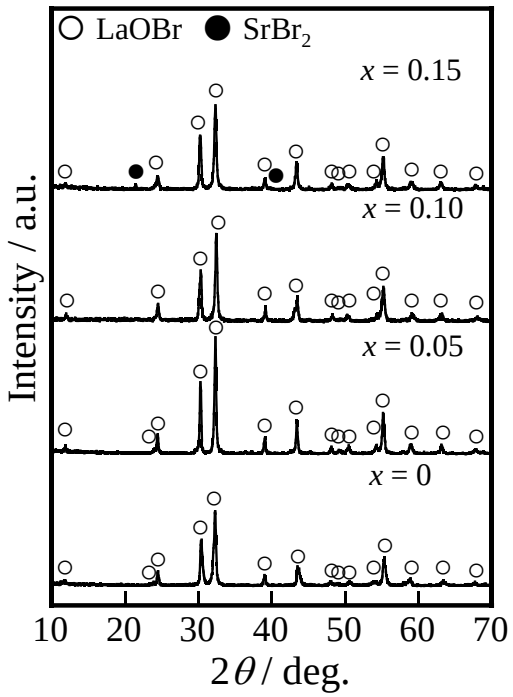

Figure 2.3. XRD patterns of the $La_{0.95-x}Sr_xCa_{0.05}OBr_{0.95-x}$ ($0 \leq x \leq 0.15$) solids.

Figure 2.4 shows the lattice volume and the electrical conductivity at 800°C for the $La_{0.95-x}Sr_xCa_{0.05}OBr_{0.95-x}$ solids as a function of Sr^{2+} ion content (x). For the samples with $x \leq 0.10$, the lattice volume increased with increasing the Sr^{2+} ion content, due to the introduction of large Sr^{2+} ion (0.140 nm, CN = 8 [8]) into the La^{3+} (0.130 nm, CN = 8 [8]) site. Moreover, the conductivity increased with increasing Sr^{2+} ion up to x = 0.10. For the sample with x = 0.15, the lattice volume was similar to the sample with x = 0.10 together with the slight decrease of conductivity; hence, the solid solubility limit of Sr (x) for the $La_{0.95-x}Sr_xCa_{0.05}OBr_{0.95-x}$ solids was found to be x = 0.10. The increase in conductivity is due to the higher amount of Br^- ion vacancies and the enlargement of the Br^- ion

conducting pathway. On the other hand, the decrease of the conductivity was due to the formation of impurity phase. From this result, it was clear that the highest conductivity was obtained for the $La_{0.85}Sr_{0.10}Ca_{0.05}OBr_{0.85}$ (x = 0.10) solid.

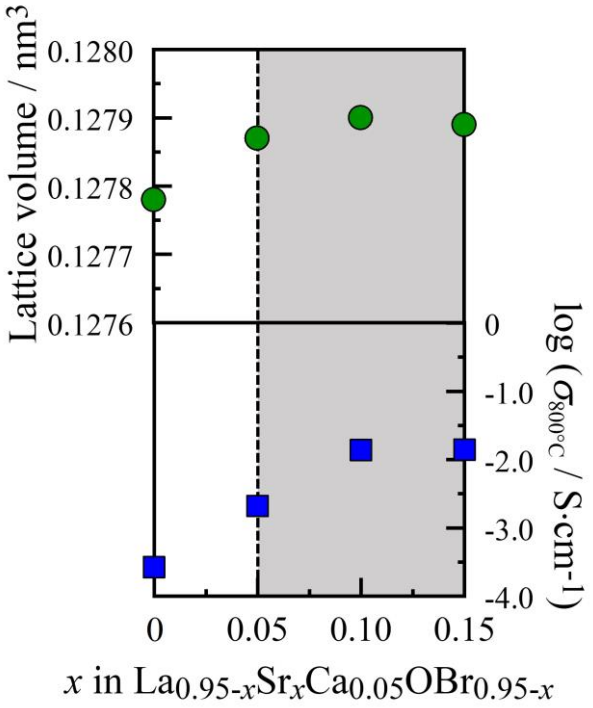

Figure 2.4. Lattice volume and conductivity at 800°C for the $La_{0.95-x}Sr_xCa_{0.05}OBr_{0.95-x}$ ($0 \leq x \leq 0.15$) solids as a function of the amount of Sr^{2+} ion content (x).

The Br^- ion migration in the $La_{0.85}Sr_{0.10}Ca_{0.05}OBr_{0.85}$ solid was investigated by the modified Tubandt electrolysis, similar to the Chapter 1. As shown in **Figure 2.5**, one La_2O_3 sample (pellet A) and two $La_{0.85}Sr_{0.10}Ca_{0.05}OBr_{0.85}$ samples (pellets B and C) were set up with two platinum blocking electrodes. The electrolysis was conducted by applying dc voltage of 0.7 V (decomposition voltage of $La_{0.85}Sr_{0.10}Ca_{0.05}OBr_{0.85}$: 0.6 V), to the sintered pellet at 700°C for 4 h. From the results for the elemental distribution in the electrolyzed pellets (**Figure 2.5**), only Br segregation was evident on and near surface of La_2O_3 pellet (A) in contact with $La_{0.85}Sr_{0.10}Ca_{0.05}OBr_{0.85}$ pellet (B), while such segregation was not recognized for other ions. This result demonstrates that the conducting ion species

in the $La_{0.85}Sr_{0.10}Ca_{0.05}OBr_{0.85}$ solid is Br^- ion. **Table 2-1** lists the observed weight changes of each pellet by the electrolysis, with the theoretical values in the case of the Br^- ion conduction. A weight increase of La_2O_3 (pellet A) was confirmed, while the sum of weight of the pellet B and C was decreased. In addition, the actual weight change values agreed with the theoretical values of Br^- anion conduction; i.e., the measured / theoretical weight ratios were ca. 87% (pellet A) and 91% (pellet B and C). Therefore, Br^- anion migration in $La_{0.85}Sr_{0.10}Ca_{0.05}OBr_{0.85}$ was quantitatively demonstrated, as same as the case for the $La_{0.90}Sr_{0.10}OBr_{0.90}$ described in Chapter 1.

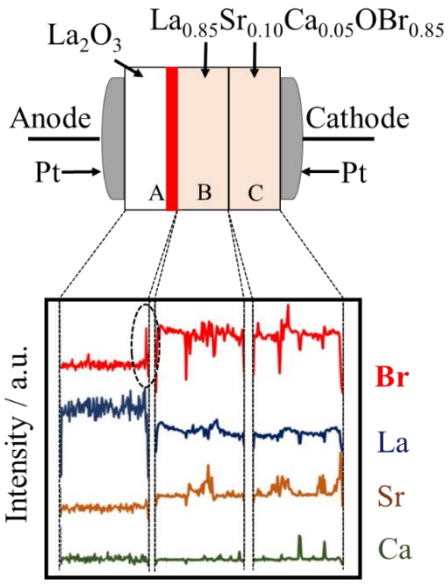

Figure 2.5. Modified Tubandt electrolysis cell using La_2O_3 and $La_{0.85}Sr_{0.10}Ca_{0.05}OBr_{0.85}$ pellets and the results of EDX line analysis after the electrolysis applied at 0.7 V, 700°C for 4 h in air.

Table 2-1. Theoretical and observed weight changes for the electrolyzed La_2O_3 (pellet A) and $La_{0.85}Sr_{0.10}Ca_{0.05}OBr_{0.85}$ (pellets B and C)

Pellet	Theoretical weight change / mg	Observed weight change / mg	Observed / theoretical weight change
A	+0.303	+0.265	87 %
B	0	−0.277	91 %
C	−0.303		

Figure 2.6 depicts the temperature dependence of the Br^- ion conductivity in the $La_{0.85}Sr_{0.10}Ca_{0.05}OBr_{0.85}$ solid (Br^- ion vacancy (δ_{Br-}) : 0.15), with the corresponding data for the $La_{0.90}Sr_{0.10}OBr_{0.90}$ (δ_{Br-} = 0.10) and LaOBr (δ_{Br-} = 0) solids. The $La_{0.85}Sr_{0.10}Ca_{0.05}OBr_{0.85}$ solid showed 5 times higher conductivity than that of the $La_{0.90}Sr_{0.10}OBr_{0.90}$ solid at 800°C, due to the formation of higher amount of Br^- ion vacancies by introducing the Ca^{2+} ion simultaneously with Sr^{2+} ion, while the activation energy (92.0 kJ·mol^{-1}) for Br^- ion conduction in the $La_{0.85}Sr_{0.10}Ca_{0.05}OBr_{0.85}$ solid was increased compared with that of $La_{0.90}Sr_{0.10}OBr_{0.90}$ solid (84.3 kJ·mol^{-1}) because of the lattice shrinkage by doping small Ca^{2+} ion.

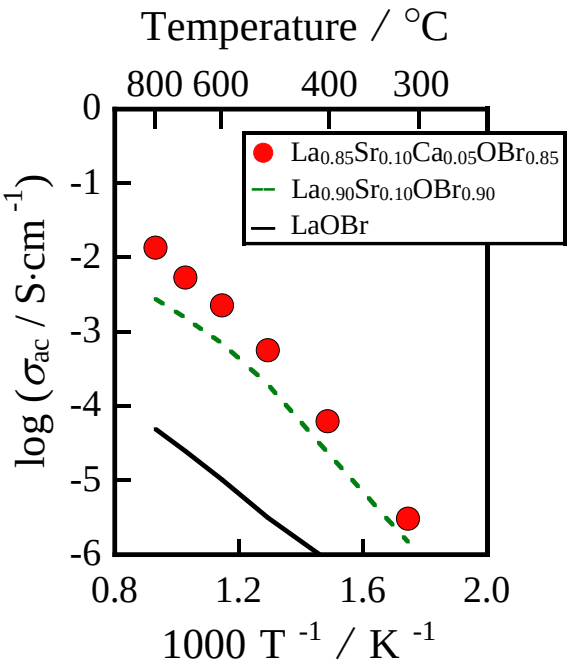

Figure 2.6. Temperature dependencies of the $La_{0.85}Sr_{0.10}Ca_{0.05}OBr_{0.85}$, $La_{0.90}Sr_{0.10}OBr_{0.90}$, and LaOBr solids.

2.4. Conclusions

In order to introduce higher amount of Br^- ion vacancies into the LaOBr solid compared with the $La_{0.90}Sr_{0.10}OBr_{0.90}$ solid with controlling the LaOBr lattice size, La^{3+} ion sites in the LaOBr were partially substituted by divalent Sr^{2+} and Ca^{2+} cations simultaneously. Among the $La_{1-x-y}Sr_xCa_yOBr_{1-x-y}$ solids prepared, $La_{0.85}Sr_{0.10}Ca_{0.05}OBr_{0.85}$ whose Br^- ion vacancies were increased than the $La_{0.90}Sr_{0.10}OBr_{0.90}$ solid showed the highest Br^- ion conductivity which was ca. 5 times higher than that of $La_{0.90}Sr_{0.10}OBr_{0.90}$ at 800°C.

Chapter 3

The Effects of Topical Structural Strain on Bromide Ion Conduction in LaOBr

3.1. Introduction

In Chapter 2, it was revealed that the simultaneous doping of Sr^{2+} and Ca^{2+} ions into the La^{3+} ion sites in the LaOBr solids realized the introduction of high amount of Br^- ion vacancies with inhibiting the lattice collapse, resulting in a higher Br^- ion conductivity. As a result of optimization of the composition, the $La_{0.85}Sr_{0.10}Ca_{0.05}OBr_{0.85}$ solid holding the single-phase of LaOBr-type structure with a large number of Br^- ion vacancies ($\delta_{Br^-} = 0.15$) exhibited the highest Br^- ion conductivity in the LaOBr-type solids examined. The outcome obtained in Chapter 2 gives us an important strategy for improving Br^- ion conductivity and, at the same time, a query for the mechanism exhibiting high Br^- ion conduction. In general, solids having large and well-ordered conducting pathway can realize high ion conduction. However, the $La_{0.85}Sr_{0.10}Ca_{0.05}OBr_{0.85}$ solid whose lattice size is smaller than that of the $La_{0.90}Sr_{0.10}OBr_{0.90}$ solid showed higher conductivity while the activation energy was high, implying that there are other factors than lattice size to affect the Br^- ion conduction in the LaOBr-type solid.

In this chapter, I focused on the electronegativity which directly/indirectly influences the bonding in the structure, and selected two divalent cations having similar ionic radius, that is, Mg^{2+} ion (0.103 nm (CN = 8 [8]), EN = 1.31 [40]) and Zn^{2+} ion (0.104 nm (CN = 8 [8]), EN = 1.64 [40]) as the co-dopant instead of Ca^{2+} ion (0.126 nm (CN = 8 [8])) in order to investigate strictly the effect of electronegativity on the Br^- ion conductivity. Therefore, the $La_{1-x-y}Sr_xM_yOBr_{1-x-y}$ (M = Mg, Zn) solids were synthesized, and the relationship between Br^- ion conduction environment in the LaOBr-type structure and Br^- ion conducting properties were investigated.

3.2. Experimental Procedure

The $La_{1-x-y}Sr_xM_yOBr_{1-x-y}$ (M = Mg, Zn) solids were prepared by a solid-state reaction method, as same as the samples described in previous chapters. As the starting materials of M doping, $M(NO_3)_2 \cdot 6H_2O$ (M = Mg, Zn) were used. After the mixed powder was preheated at 850°C for 12 h under the flow of synthetic air, the obtained powder was pressed into a pellet shape and calcined at 850°C for 12 h several times to obtain the single-phase sample.

The samples obtained were identified by X-ray powder diffraction (XRD; SmartLab, Rigaku) with Cu-Kα radiation (40 kV, 30 mA) in the 2θ range from 10 to 70 degree with a scan speed of 8 degree·min^{-1} and step width of 0.04 degree. The lattice volume was estimated by refining the XRD peak angles using α-Al_2O_3 as an internal standard. To determine the structural parameters, XRD data (MultiFlex, Rigaku) were also collected using the step scanning technique (step width: 0.01 degree, count time: 3 seconds 2θ range: 10-130 degree) with Cu-Kα radiation (40 kV, 40 mA), and the obtained pattern was refined by Rietveld method with the Fullprof program [41]. Schematic crystal structure was drawn by VESTA program [42] with the refined data. X-ray photoelectron spectroscopy (XPS; PHI5000 Versa Probe II, ULVAC-PHI Corporation) was measured at room temperature with Al-Kα radiation. The charging effect on the binding energies was corrected with respect to the C 1s peak at 284.6 eV. The spectrum was fitted using a Shirley background and Gaussian-Lorentzian line shapes.

For the electrical conductivity measurements, the sample powder was pressed into a pellet shape and sintered at 850°C for 12 h in synthetic air flow. Thereafter, the platinum-sputtered layers were formed on the center surfaces of the sintered pellet polished with waterproof abrasive papers using an ion coater (IB-3, Eiko), followed by applying platinum paste on the sputtered layer. Ac conductivity (σ_{ac}) measurement of the sample pellet was conducted by a complex impedance method in the frequency range of 5 Hz to 13 MHz (1260 Impedance/Gain-Phase Analyzer, Solartron) at the temperature range of 800 to 300°C in the atmospheric air.

Modified Tubandt electrolysis was also performed for the $La_{0.80}Sr_{0.15}Mg_{0.05}OBr_{0.80}$ sintered pellet by applying a dc voltage of 1.0 V at 800°C for 4 h in the atmospheric air. The weight change and the elemental distribution in the electrolyzed pellets were confirmed with similar method described in Chapters 1 and 2.

3.3. Results and Discussions

From the XRD measurements for the $La_{1-x-y}Sr_xM_yOBr_{1-x-y}$ (M = Mg, Zn) solids by changing the Sr and M contents (*x* and *y*), it was found that the solid soluble concentration of M^{2+} ion into the La^{3+} ion site was $y = 0.05$, regardless of the Sr^{2+} ion doping amount (*x*). This might be due to the large difference in ionic radius between M^{2+} ion (Mg: 0.103 nm (CN = 8 [8]), Zn: 0.104 nm (CN = 8 [8])) and La^{3+} ion (0.130 nm (CN = 8 [8])), i.e. only few amounts of M^{2+} ion can substitute for the La^{3+} ion site for holding the crystal structure stably. Therefore, the doping amount of M^{2+} ion (M = Mg, Zn) (*y*) was fixed to $y = 0.05$ for further investigation.

Figure 3.1 shows the XRD patterns of the $La_{0.95-x}Sr_xM_{0.05}OBr_{0.95-x}$ (M = Mg, Zn; $0.10 \leq x \leq 0.20$) solids. For both the $La_{0.95-x}Sr_xMg_{0.05}OBr_{0.95-x}$ and $La_{0.95-x}Sr_xZn_{0.05}OBr_{0.95-x}$ solids, it was found that the single-phase of LaOBr-type solid was successfully obtained only for the samples with $x \leq 0.15$, while the solid with $x = 0.20$ was the two-phase mixture of LaOBr-type solid and $SrBr_2$. **Figure 3.2** displays the compositional dependence of the lattice volume for the $La_{0.95-x}Sr_xM_{0.05}OBr_{0.95-x}$ (M = Mg, Zn; $0.10 \leq x \leq 0.20$) solids. In the compositional region where the single-phase samples were obtained ($x \leq 0.15$), the lattice volume increased with increasing Sr^{2+} ion content, suggesting that the larger Sr^{2+} ion (0.140 nm, CN = 8 [8]) substituted for the La^{3+} ion (0.130 nm, CN = 8 [8]) site. On the other hand, the lattice volume of the LaOBr-type phase in the sample with $x = 0.20$ was similar to that of the sample with $x = 0.15$, indicating that the solid solubility limit composition of Sr (*x*) for

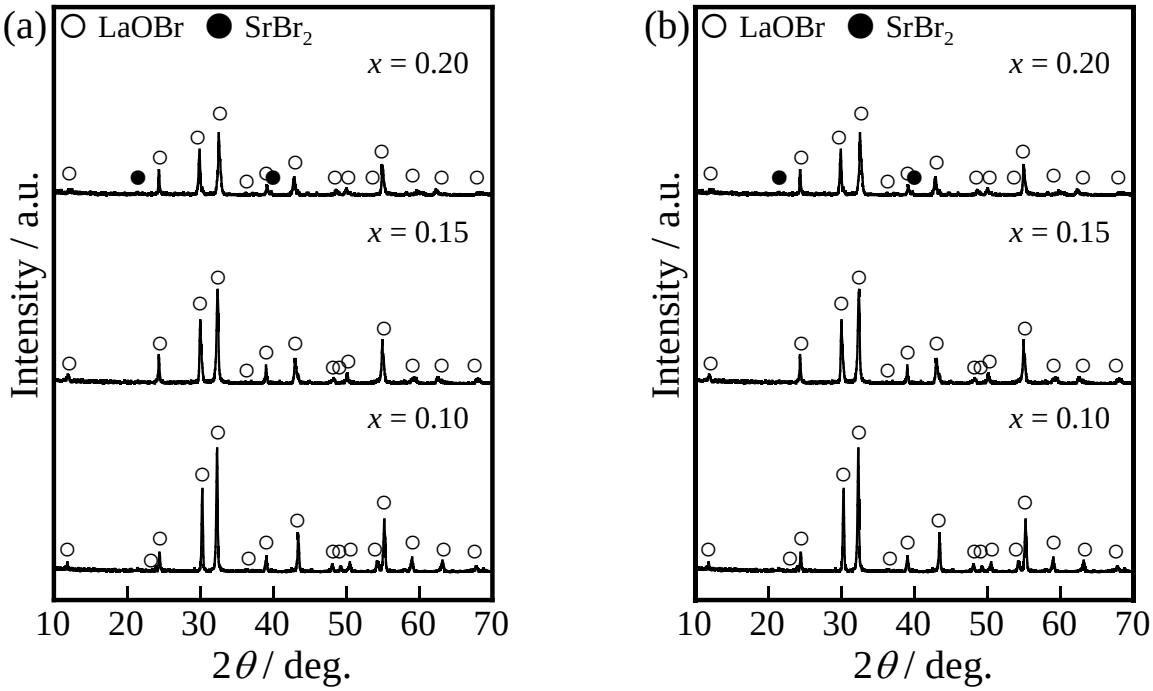

Figure 3.1. XRD patterns of the $La_{0.95-x}Sr_xM_{0.05}OBr_{0.95-x}$ (M = (a) Mg, (b) Zn; $0.10 \leq x \leq 0.20$) solids.

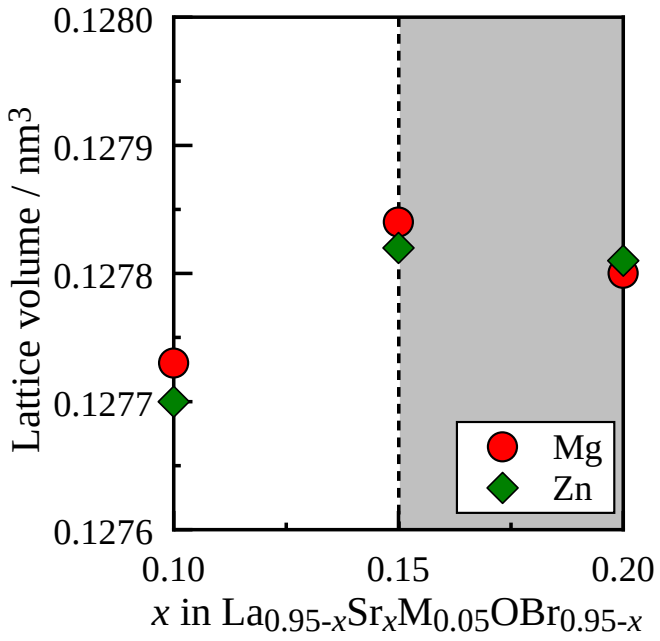

Figure 3.2. Compositional dependence of lattice volume for the $La_{0.95-x}Sr_xM_{0.05}OBr_{0.95-x}$ (M = Mg (●), Zn (♦) ($0.10 \leq x \leq 0.20$) solids.

the $La_{0.95-x}Sr_xM_{0.05}OBr_{0.95-x}$ (M = Mg, Zn; $0.10 \leq x \leq 0.20$) solids was $x = 0.15$, i.e. $La_{0.80}Sr_{0.15}M_{0.05}OBr_{0.80}$ (M = Mg, Zn). Moreover, by selecting smaller Mg^{2+} or Zn^{2+} ion than Ca^{2+} ion (Chapter 2) as the co-dopant cation with Sr^{2+} ion, the limit concentration of the Br^- ion vacancy which can be introduce into the LaOBr structure was successfully increased than the Ca-doped $La_{0.95-x}Sr_xCa_{0.05}OBr_{0.95-x}$ solid (solid solubility limit: $x = 0.10$). By comparing the lattice volume for both systems in the single-phase region, Mg-doped solids have larger lattice volume while the ionic size of Mg^{2+} ion is slightly smaller than the Zn^{2+} ion, which is quite strange result expected from the substitutional-type solid solution.

Figure 3.3 depicts the ac conductivity at 800°C and the activation energy for the $La_{0.95-x}Sr_xM_{0.05}OBr_{0.95-x}$ (M = Mg, Zn; $0.10 \leq x \leq 0.20$) solids as a function of Sr^{2+} ion content (x). In the single-phase region ($x \leq 0.15$), the conductivity enhanced and the activation energy lowered with increasing x. The increase of the conductivity and the decrease of the activation energy are mainly

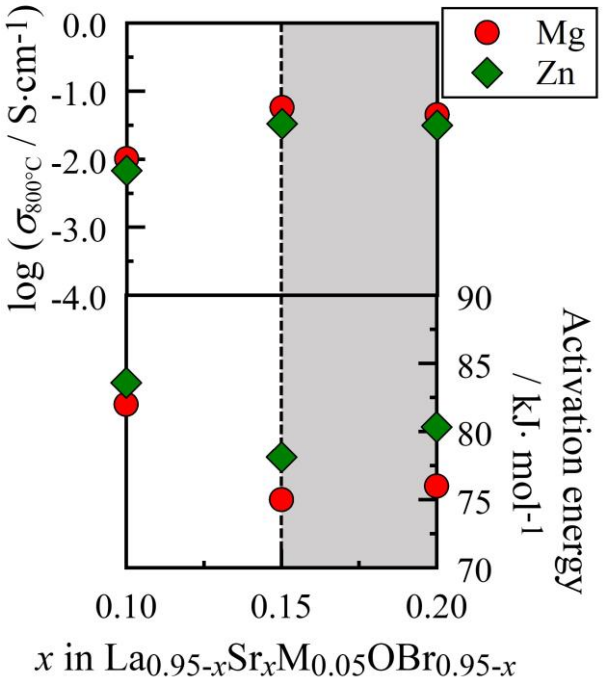

Figure 3.3. Ac conductivity and activation energy for the $La_{0.95-x}Sr_xM_{0.05}OBr_{0.95-x}$ (M = Mg (●), Zn (♦) ($0.10 \leq x \leq 0.20$) solids as a function of Sr^{2+} ion content (x).

attributed to the increase of the Br^- ion vacancies as well as the expansion of the Br^- ion migration pathway due to the replacement of the La^{3+} ion site with Sr^{2+} ion having the lower-valence state and larger ionic radius. For the x = 0.20 sample, the conductivity decreased and the activation energy increased compared to the sample with x = 0.15, owing to the formation of impurity phase of $SrBr_2$. Therefore, the highest conductivity and the lowest activation energy were obtained simultaneously for the $La_{0.80}Sr_{0.15}M_{0.05}OBr_{0.80}$ (M = Mg, Zn; x = 0.15) solids.

As mentioned above, upon comparing the sample with the same composition in the single-phase region, it was found that the lattice volume of the Mg-doped sample was larger than that of the Zn-doped sample, even though the ionic radius of Mg^{2+} ion is smaller than Zn^{2+} ion. This result implies the existence of other factors contributing to the change of lattice size than the ionic size of dopant. Therefore, the structural analysis of the $La_{0.80}Sr_{0.15}M_{0.05}OBr_{0.80}$ (M = Mg, Zn) solids were conducted. **Figure 3.4** shows the results of Rietveld refinements for the XRD patterns (step width: 0.01 degree, count time: 3 seconds) of the $La_{0.80}Sr_{0.15}M_{0.05}OBr_{0.80}$ (M = Mg, Zn; x = 0.15) solids, and the structural parameters including lattice constants of these solids are summarized in **Table 3.1**. As drawn in **Figure 3.5**, the LaOBr-type structure is the tetragonal layered structure of which Br layer is sandwiched by

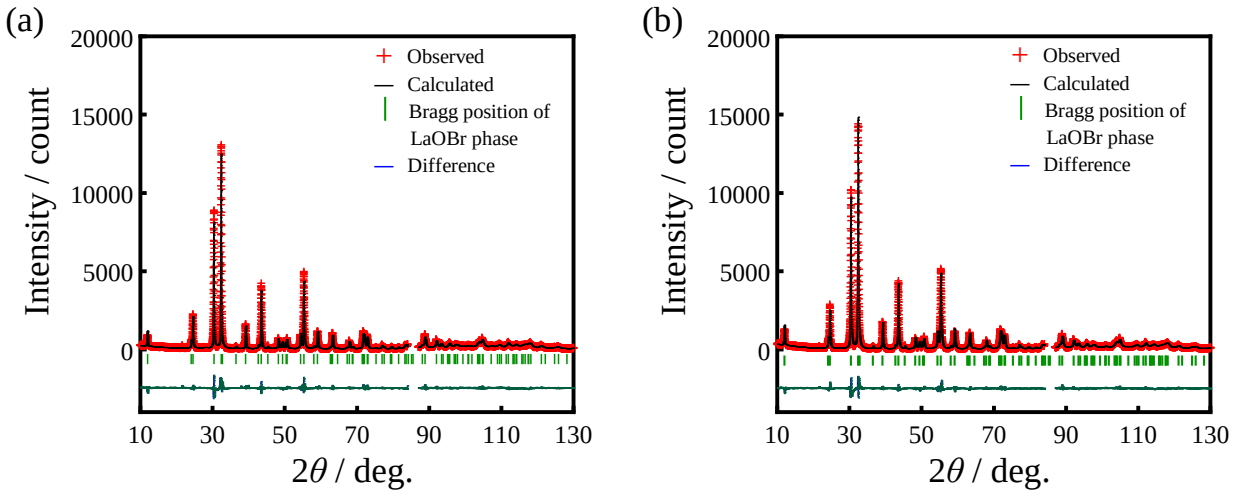

Figure 3.4. Results of the Rietveld refinements of the XRD data for the $La_{0.80}Sr_{0.15}M_{0.05}OBr_{0.80}$ (M = (a) Mg, (b) Zn) solids.

Table 3.1. Structural parameters determined by the Rietveld refinements for the XRD (Cu-Kα) patterns of the $La_{0.80}Sr_{0.15}M_{0.05}OBr_{0.80}$ (M = Mg, Zn) solids at room temperature.

Sample	Atom	Wyckoff position	*g*	*x*	*y*	*z*	*B* / Å^2
$La_{0.80}Sr_{0.15}Mg_{0.05}OBr_{0.80}$	La	2*c*	0.80	0	0.5	0.1631(1)	0.582(3)
	Sr	2*c*	0.15	0	0.5	= *z*(La)	= *B*(La)
	Mg	2*c*	0.05	0	0.5	= *z*(La)	= *B*(La)
	O	2*a*	1.00	0	0	0	0.510(3)
	Br	2*c*	0.80	0	0.5	0.6214 (2)	0.691(1)
Tetragonal (*P*4/*nmm*, No. 129), *a* = 0.4190(1) nm, *c* = 0.7291(3) nm, α = β = γ = 90°, *Z* = 2 R_{wp} = 15.1 %, *S* = 1.57							
$La_{0.80}Sr_{0.15}Zn_{0.05}OBr_{0.80}$	La	2*c*	0.80	0	0.5	0.1624(1)	0.565(2)
	Sr	2*c*	0.15	0	0.5	= *z*(La)	= *B*(La)
	Zn	2*c*	0.05	0	0.5	= *z*(La)	= *B*(La)
	O	2*a*	1.00	0	0	0	0.588(3)
	Br	2*c*	0.80	0	0.5	0.6263(2)	0.712(3)
Tetragonal (*P*4/*nmm*, No. 129), *a* = 0.4182(2) nm, *c* = 0.7307(1) nm, α = β = γ = 90°, *Z* = 2 R_{wp} = 14.1 %, *S* = 1.62							

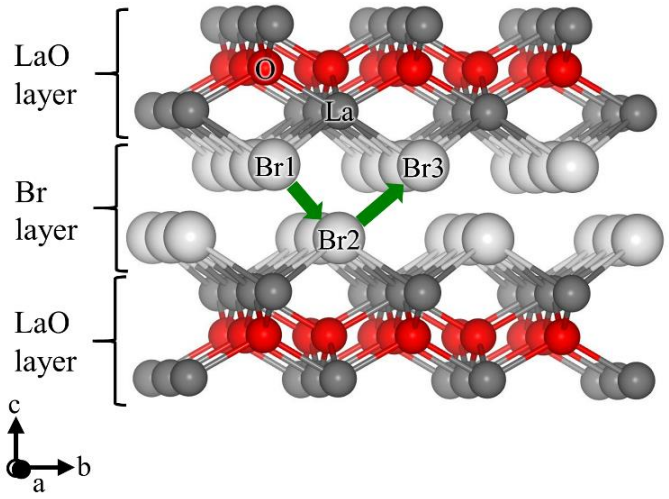

Figure 3.5. The schematic drawing of the LaOBr-type structure with the proposed Br^- ion migrating pathway shown as green arrows [43].

Table 3.2. The average distances of O-La ($d_{O\text{-}La}$), Br1-La ($d_{Br1\text{-}La}$), Br2-La ($d_{Br2\text{-}La}$), Br1-Br2 ($d_{Br1\text{-}Br2}$) and Br1-Br3 ($d_{Br1\text{-}Br3}$), and the average angle of Br1-Br2-Br3 ($\phi_{Br1\text{-}Br2\text{-}Br3}$) determined by Rietveld analyses for the $La_{0.80}Sr_{0.15}M_{0.05}OBr_{0.80}$ (M = Mg, Zn) solids.

Sample	$d_{O\text{-}La}$ / nm	$d_{Br1\text{-}La}$ / nm	$d_{Br2\text{-}La}$ / nm	$d_{Br1\text{-}Br2}$ / nm	$d_{Br1\text{-}Br3}$ / nm	$\phi_{Br1\text{-}Br2\text{-}Br3}$ / deg.
$La_{0.80}Sr_{0.15}Mg_{0.05}OBr_{0.80}$	0.2409(1)	0.3354(1)	0.3342(1)	0.3451(1)	0.4190(1)	74.75(1)
$La_{0.80}Sr_{0.15}Zn_{0.05}OBr_{0.80}$	0.2404(1)	0.3336(1)	0.3390(1)	0.3486(1)	0.4182(1)	73.72(1)

fluorite-type LaO layers. The distances of O–La ($d_{O–La}$), Br1–La ($d_{Br1–La}$), Br2–La ($d_{Br2–La}$), Br1–Br2 ($d_{Br1–Br2}$), and Br1–Br3 ($d_{Br1–Br3}$), and the angle for Br1–Br2–Br3 ($\phi_{Br1–Br2–Br3}$) were estimated by using VESTA program [42] and are summarized in **Table 3.2**. Here, Br in **Figure 3.5** is denoted in distinction; e.g., Br1 and Br3 bond to the same La, while Br2 bonds with another La, for the purpose of discussing Br^- migration in the solid. From the lattice parameters listed in **Table 3.1**, the $La_{0.80}Sr_{0.15}Mg_{0.05}OBr_{0.80}$ solid has larger *a* and smaller *c* compared to those of the $La_{0.80}Sr_{0.15}Zn_{0.05}OBr_{0.80}$ solid. Since LaOBr consists of rigid fluorite-type LaO layers, the length of *a* and *b* axes are determined by the La–O bond length. The partial substitution of Mg having comparatively lower electronegativity (1.31 [40]) than Zn (1.64 [40]) into the La^{3+} ion site caused weaker La–O bond strength, and the La–O distance elongates. The expansion of LaO layer toward *a* and *b* direction also involved with the displacement of Br, where the distance between Br1 and Br3 increases. Due to the relaxation of the lattice distortion resulted from the LaO layer expansion, the lattice parameter *c* decreases. Consequently, the distance between Br1 and Br2 ($d_{Br1–Br2}$) associated with the proposed Br^- ion conduction pathway [43] in the $La_{0.80}Sr_{0.15}Mg_{0.05}OBr_{0.80}$ solid was shorter than that of the $La_{0.80}Sr_{0.15}Zn_{0.05}OBr_{0.80}$ solid, meaning the shortening of the Br^- ion conducting path. In addition, $La_{0.80}Sr_{0.15}Mg_{0.05}OBr_{0.80}$ showed wider average angle of Br1–Br2–Br3 ($\phi_{Br1–Br2–Br3}$) compared to $La_{0.80}Sr_{0.15}Zn_{0.05}OBr_{0.80}$, which is considered efficient for smooth Br^- anion conduction in the Br layer. Furthermore, the La–Br bond strength should be different for the solids doped with Mg

and Zn, because the electronegativity of cation affects the bond covalency and/or ionicity. Therefore, the La–Br bond strength was investigated by calculating the bond valence sum (BVS) using VESTA program [42]. The La–Br bond strength for $La_{0.80}Sr_{0.15}Mg_{0.05}OBr_{0.80}$ (BVS = 0.755) was weaker than that of (0.768) for the $La_{0.80}Sr_{0.15}Zn_{0.05}OBr_{0.80}$ solid, which is considered to facilitate the bond cleavage for Br^- ion migration. This difference in bond strength was also supported by XPS measurement.

Figure 3.6 shows the Br 3d and O 1s XPS spectra for the $La_{0.80}Sr_{0.15}M_{0.05}OBr_{0.80}$ (M = Mg, Zn) solids. The doublet peaks of Br $3d_{3/2}$ (ca. 69.8 eV) and $3d_{5/2}$ (ca. 68.7 eV) peaks were observed, as shown in **Figure 3.6(a)**. In the case of the O 1s (**Figure 3.6(b)**), the peak at ca. 529 eV is identified as the lattice oxygen, while the others relate to the surface oxygen species such as adsorbed oxygen (ca. 531 eV) and the surface hydroxyl species and/or adsorbed water (ca. 533 eV) [44]. The Br and O peaks of the $La_{0.80}Sr_{0.15}Mg_{0.05}OBr_{0.80}$ were shifted toward the lower binding energy compared to those of $La_{0.80}Sr_{0.15}Zn_{0.05}OBr_{0.80}$, indicating that the electron density of these anions in the $La_{0.80}Sr_{0.15}Mg_{0.05}OBr_{0.80}$ solid are higher than those in $La_{0.80}Sr_{0.15}Zn_{0.05}OBr_{0.80}$. High electron density

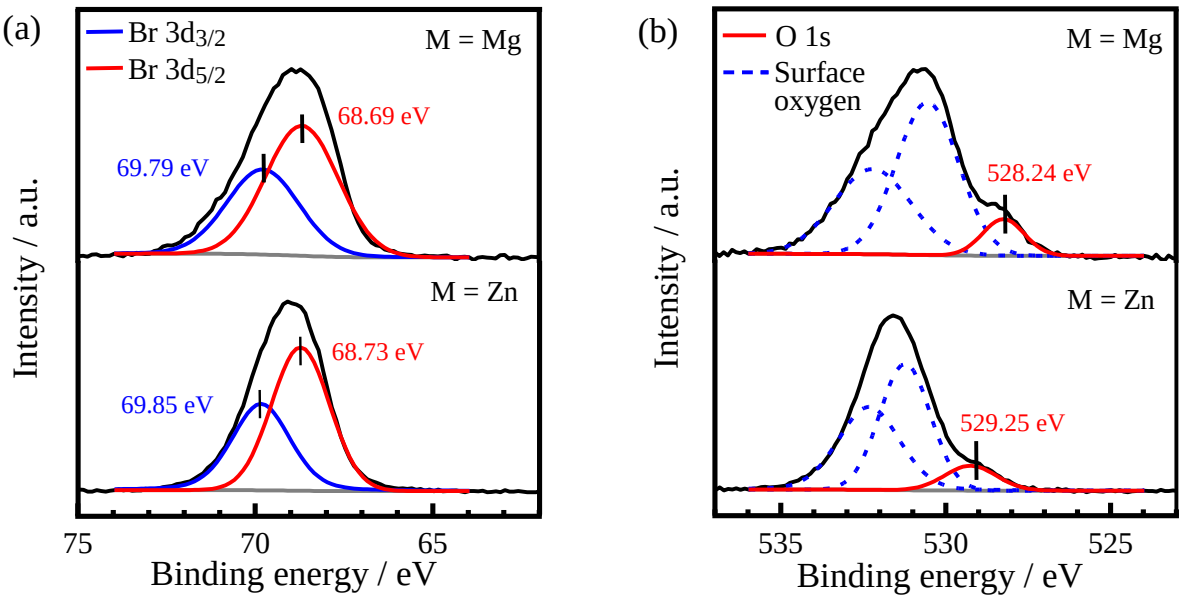

Figure 3.6. XPS spectra of (a) Br 3d and (b) O 1s core-levels of the $La_{0.80}Sr_{0.15}M_{0.05}OBr_{0.80}$ (M = Mg, Zn) solids.

of anions attributed to increase of ionicity. In general, ionic bonding is weaker than the covalent one due to the polarization of electron between elements. The weak bonding was considered to elongate the bond length and facilitate the bond cleavage, which supports the result of the crystal structural analysis.

Based on the results from the structural analysis and XPS, it was revealed that Mg having the relatively low electronegativity compared to Zn weakened the bond strength between Br and La site and shorten the Br^- ion conducting pathway, resulting in the higher conductivity and lower activation energy for $La_{0.80}Sr_{0.15}Mg_{0.05}OBr_{0.80}$ compared to $La_{0.80}Sr_{0.15}Zn_{0.05}OBr_{0.80}$.

The Br^- ion migration in the $La_{0.80}Sr_{0.15}Mg_{0.05}OBr_{0.80}$ solid was investigated by the modified Tubandt electrolysis (**Figure 3.7**), similar to Chapters 1 and 2. The electrolysis was conducted by applying a dc voltage of 1.0 V (decomposition voltage of $La_{0.80}Sr_{0.15}Mg_{0.05}OBr_{0.80}$: 0.9 V), to the sintered pellet at 800°C for 4 h. Based on the elemental distribution inside the electrolyzed pellets,

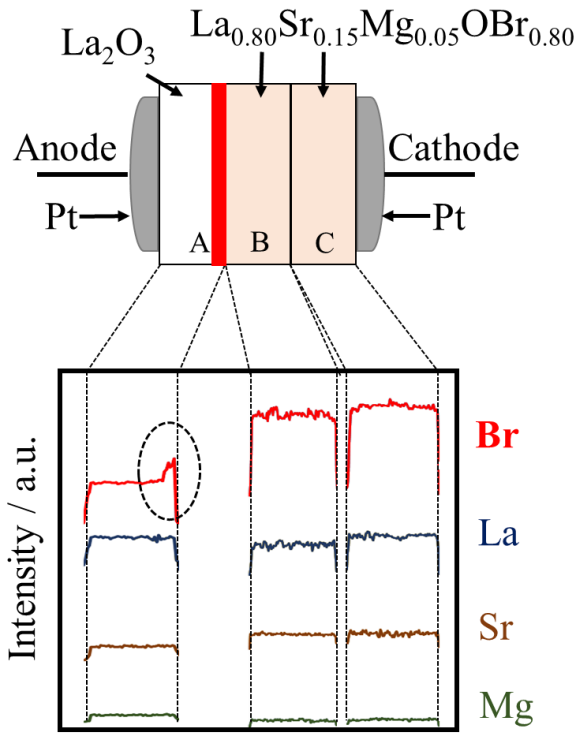

Figure 3.7. Modified Tubandt electrolysis cell with the La_2O_3 and $La_{0.80}Sr_{0.15}Mg_{0.05}OBr_{0.80}$ pellets and the results of EDX line analysis after the electrolysis applied at 1.0 V, 800°C for 4 h in air.

only segregation of Br was evident on and near surface of La_2O_3 pellet (pellet A) in contact with $La_{0.80}Sr_{0.15}Mg_{0.05}OBr_{0.80}$ pellet (pellet B). This result demonstrates that the migrating ion species in the $La_{0.80}Sr_{0.15}Mg_{0.05}OBr_{0.80}$ solid is Br^- ion. **Table 3-3** lists the observed weight changes of respective pellet after the electrolysis, with the theoretical values in the case of the Br^- ion conduction. A weight increase of La_2O_3 (pellet A) and the weight decrease of the pellet B and C were observed. In addition, the actual weight change values were almost the same as the theoretical values of Br^- anion conduction; i.e., the measured / theoretical weight ratios were ca. 96% (pellet A) and 97% (pellet B and C). Therefore, Br^- anion migration in $La_{0.80}Sr_{0.15}Mg_{0.05}OBr_{0.80}$ was quantitatively demonstrated.

Table 3-3. Theoretical and observed weight changes for the electrolyzed La_2O_3 (pellet A) and $La_{0.80}Sr_{0.15}Mg_{0.05}OBr_{0.80}$ (pellets B and C)

Pellet	Theoretical weight change / mg		Observed weight change / mg	Observed / theoretical weight change
A	+0.155		+0.149	96 %
B	0	}	−0.151	97 %
C	−0.155			

Figure 3.8 depicts the temperature dependence of the Br^- ion conductivity for the $La_{0.80}Sr_{0.15}Mg_{0.05}OBr_{0.80}$ solid (amount of Br^- ion vacancy (δ_{Br-}) = 0.20), with the corresponding data for $La_{0.85}Sr_{0.10}Ca_{0.05}OBr_{0.85}$ (δ_{Br-} = 0.15), $La_{0.90}Sr_{0.10}OBr_{0.90}$ (δ_{Br-} = 0.10) and LaOBr. The $La_{0.80}Sr_{0.15}Mg_{0.05}OBr_{0.80}$ solid showed the highest Br^- ion conductivity and the lowest activation energy among the solids investigated, due to the introduction of the highest amount of Br^- ion vacancy as listed in **Table 3-4**, regardless of the smallest lattice volume. This result indicates that the Br^- ion migration in the LaOBr-type structure is largely influenced by the amount of Br^- ion vacancies compared with the lattice volume. Moreover, from the result of investigation for the

$La_{0.80}Sr_{0.15}M_{0.05}OBr_{0.80}$ (M = Mg, Zn) solids, adjustment of electronegativity can improve the Br^- ion conductivity in the LaOBr-type solid by the elongation of La–Br distance even if the lattice size becomes small.

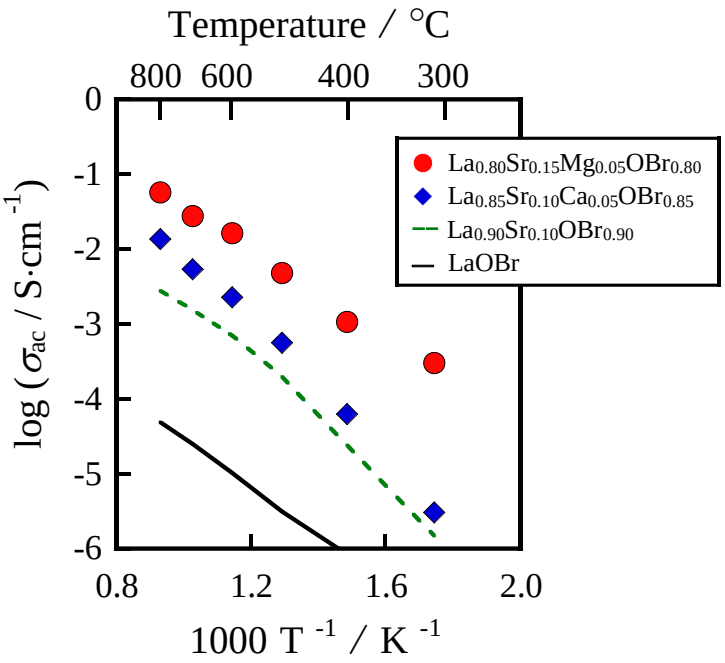

Figure 3.9. Temperature dependencies of the $La_{0.80}Sr_{0.15}Mg_{0.05}OBr_{0.80}$, $La_{0.85}Sr_{0.10}Ca_{0.05}OBr_{0.85}$, $La_{0.90}Sr_{0.10}OBr_{0.90}$, and LaOBr solids.

Table 3-4. Br^- ion vacancy concentration, lattice volume, Br^- ion conductivity and activation energy for Br^- ion conduction for the $La_{0.80}Sr_{0.15}Mg_{0.05}OBr_{0.80}$, $La_{0.85}Sr_{0.10}Ca_{0.05}OBr_{0.85}$, and $La_{0.90}Sr_{0.10}OBr_{0.90}$ solids

Solid	Br^- ion vacancy concentration	Lattice volume / nm^3	Conductivity at 800°C / S·cm^{-1}	Activation energy / kJ·mol^{-1}
$La_{0.80}Sr_{0.15}Mg_{0.05}OBr_{0.80}$	0.20	0.1278	6.5×10^{-2}	78
$La_{0.85}Sr_{0.10}Ca_{0.05}OBr_{0.85}$	0.15	0.1279	1.4×10^{-2}	92
$La_{0.90}Sr_{0.10}OBr_{0.90}$	0.10	0.1281	2.8×10^{-3}	84

3.4. Conclusions

In order to investigate strictly the factors that affect the Br^- ion conduction in the LaOBr-type solid other than the lattice volume, Mg^{2+} and Zn^{2+} ions having similar ionic radius and different electronegativity were selected as the co-dopant together with Sr^{2+} ions into the $La_{1-x-y}Sr_xM_yOBr_{1-x-y}$ (M = Mg, Zn) solids. From the structural analysis of the $La_{0.80}Sr_{0.15}M_{0.05}OBr_{0.80}$ (M = Mg, Zn) solids having the same amount of Br^- ion vacancies, it was found that Mg having the lower electronegativity weaken the bond strength between Br and La site and shorten the Br^- ion conducting path. From this result, it is revealed that the Br^- ion migration in the LaOBr-type structure is greatly influenced by both the amount of Br^- ion vacancies and the circumstance of the conducting pathway in the structure which can be controlled by adjusting the ionic size and electronegativity of doping cations.

Summary

In the study of this thesis, the key factors contributing to the Br^- ion conducting properties in lanthanum oxybromide, LaOBr were clarified.

The results and conclusions obtained through this work are summarized as follows:

Chapter 1

For clarifying the effects of Br^- ion vacancy and lattice size on the Br^- ion conduction in the LaOBr-type structure, the La^{3+} ions in the LaOBr were partially replaced for various alkaline earth metal cations. The introduction of divalent cations enhanced the conductivity of LaOBr caused by the formation of Br^- ion vacancies. In addition, since the conductivity enhanced with increasing lattice volume, it was clarified that the enhancement of the Br^- ion conductivity was achieved by the introduction of Br^- ion vacancy and the enlargement of Br^- ion conducting pathway.

Chapter 2

For improving the Br^- ion conductivity of the $La_{0.90}Sr_{0.10}OBr_{0.90}$ solid, the Sr^{2+} ion was doped together with smaller ionic-radius of Ca^{2+} ion to introduce higher amount of Br^- ion vacancy in the LaOBr structure with the intentional control of the lattice size. Co-doping of Ca^{2+} realized the inhibition of lattice collapse caused by the generation of higher amount of Br^- ion vacancy, and the $La_{0.85}Sr_{0.10}Ca_{0.05}OBr_{0.85}$ solid (δ_{Br^-} = 0.15) whose Br^- ion vacancies were increased than the $La_{0.90}Sr_{0.10}OBr_{0.90}$ (δ_{Br^-} = 0.10) solid exhibited the highest Br^- ion conductivity which was ca. 5 times higher than that of $La_{0.90}Sr_{0.10}OBr_{0.90}$ at 800°C.

Chapter 3

For discussing the relationship between the local structural change of LaOBr lattice and the

Br^- ion conducting property, Mg^{2+} and Zn^{2+} whose electronegativity was quite different were selected as the co-dopant species of the Sr^{2+} ion. From the detail structural analysis, doping of the Mg with lower electronegativity was demonstrated to weaken the bond strength between Br and La, which facilitates the La−Br bond cleavage and shorten the Br^- ion conduction path. Such a local structural strain highly contributed to the improvement of the Br^- ion conduction. The results obtained in this study revealed that the Br^- ion conduction in the LaOBr-type solids was determined by both the amount of Br^- ion vacancies and the Br^- ion conducting environment in the lattice which can be controlled by strict selection of the ionic size as well as the electronegativity of the dopant cations.

References

[1] C. Wang, K. Fu, S.P. Kammampata, D.W. McOwen, A.J. Samson, L. Zhang, G.T. Hitz, A.M. Nolan, E.D. Wachsman, Y. Mo, V. Thangadurai, and L. Hu, *Chem. Rev.*, **120**, 4257-4300 (2020).

[2] Q. Zhao, S. Stalin, C.Z. Zhao, and L.A. Archer, *Nat. Rev. Mater.*, **5**, 229-252 (2020).

[3] Z. Zakaria, Z.A. Mat, S.H.A. Hassan, and Y.B. Kar, *Int. J. Energy Res.*, **44**, 594-611 (2020).

[4] T. Krauskopf, F.H. Richter, W.G. Zeier, and J. Janek, *Chem. Rev.*, **120**, 7745-7794 (2020).

[5] D.H.S. Tan, A. Benerjee, Z. Chen, and Y.S. Meng, *Nat. Nanotech.*, **15**, 170-180 (2020).

[6] S. Mulmi and V. Thangadurai, *J. Electrochem. Soc.*, **167**, 037567:1-14 (2020).

[7] T.K. Schwietert, V.A. Arszelewska, C. Wang, C. Yu, A. Vasileiadis, N.J.J. de Klerk, J. Hageman, T. Hupfer, I. Kerkamm, Y. Xu, E. van der Maas, E.M. Kelder, S. Ganapathy, and M. Wagemaker, *Nat. Mater.*, **19**, 428-435 (2020).

[8] R.D. Shannon, *Acta Crystallogr.*, **A32**, 751-769 (1976).

[9] T. Teranishi, A. Kouchi, H. Hayashi, and A. Kishimoto, *Solid State Ionics*, **263**, 33-40 (2014).

[10] N. Kamaya, K. Honma, Y. Yamakawa, M. Hirayama, R. Kanno, M. Yonemura, T. Kamiyama, Y. Kato, S. Hama, K. Kawamoto, and A. Mitsui, *Nat. Mater.*, **10**, 677-682 (2011).

[11] P. Bron, S. Johansson, K. Zick, K.J. auf der Gunne, S. Dehnen, and B. Roling, *J. Am. Chem. Soc.*, **135**, 15694-15699 (2013).

[12] A. Haffner, A.K. Hatz, I. Moudrakovski, B.V. Lotsch, and D. Johrendt, *Angew. Chem., Int. Ed.*, **57**, 6155-6160 (2018).

[13] A. Hayashi, N. Masuzawa, S. Yubuchi, F. Tsuji, C. Hotehama, A. Sakuda, and M. Tatsumisago, *Nat. Commun.*, **10**, 5266:1-4 (2019).

[14] W.D. Richards, T. Tsujimura, L.J. Miara, Y. Wang, J.C. Kim, S.P. Ong, I. Uechi, N. Suzuki, and G. Ceder, *Nat. Commun.*, **7**, 11009:1-8 (2016).

[15] C. Rongeat, M.A. Reddy, R. Witter, and M. Fichtner, *ACS Appl. Mater. Interfaces*, **6**, 2103-

2110 (2014).

[16] I. Mohammad, J. Chable, R. Witter, M. Fichtner, and M.A. Reddy, *ACS Appl. Mater. Interfaces*, **10**, 17249-17256 (2018).

[17] K. Mori, A. Mineshige, T. Saito, M. Sugiura, Y. Ishikawa, F. Fujisaki, K. Namba, T. Kamiyama, T. Otomo, T. Abe, and T. Fukunaga, *ACS Appl. Mater. Interfaces*, **3**, 2873-2880 (2020).

[18] S. Tamura, M. Yamane, Y. Hoshino, and N. Imanaka, *J. Solid State Chem.*, **235**, 7-11 (2016).

[19] S.S. Park, Y. Tulchinsky, and M. Dincă, *J. Am. Chem. Soc.*, **139**, 13260-13263 (2017).

[20] R.L. Ruyet, R. Berthelot, A. Salager, P. Florian, B. Fleutot, and R. Janot, *J. Phys. Chem. C*, **123**, 10756-10763 (2019).

[21] K. Nomura, S. Ikeda, K. Ito, and H. Einaga, *Bull. Chem. Soc. Jpn.*, **65**, 3221-3227 (1992).

[22] W. Lee, S. Tamura, and N. Imanaka, *Chem. Lett.*, **46**, 1486-1489 (2017).

[23] Q. Yang, M. Zhang, C. Ming, G. Liu, and M. Wang, *Int. J. Electrochem. Sci.*, **14**, 4933-4945 (2019).

[24] D.W. Strickler and W.G. Carlson, *J. Am. Ceram. Soc.*, **47**, 122-127 (1964).

[25] J.J. Biendicho, H.Y. Playford, S.M.H. Rahman, S.T. Norberg, S.G. Eriksson, and S. Hull, *Inorg. Chem.*, **57**, 7025-7035 (2018).

[26] L. Sévin, V. Razifindramanana, A. Julian-Jankowiak, J.F. Justin, F. Mauvy, and F. Rebillat, *J. Eur. Ceram. Soc.*, **40**, 5859-5869 (2020).

[27] J. Mizusaki, K. Arai, and K. Fueki, *Solid State Ionics*, **11**, 203-11 (1983).

[28] H. Aono and E. Sugimoto, *Chem. Lett.*, **24,** 79-79 (1995).

[29] V.E. Distanov and V.A. Drebushchak, *J. Therm. Anal. Calorim.*, **57**, 599-605 (1999).

[30] C.Y. Huang, C.C. Wu, C.L. Wu, and C.W. Lin, *ACS Omega*, **4**, 8081-8086 (2019).

[31] A. Seidell, *Solubilities of Inorganic and Organic Compounds 2nd Edition*, D. Van Nostrand Company, New York, pp. 349-366 (1919).

[32] I.Y. Zaitseva, I.S. Kovaleva, and V.A. Fedorov, *Russ. J. Inorg. Chem.*, **52**, 1968-1970 (2007).

[33] I. Mayer, S. Zolotov, and F. Kassierer, *Inorg. Chem.*, **4**, 1637-1639 (1965).

[34] I. Mayer and S. Zolotov, *J. Inorg. Nucl. Chem.*, **27**, 1905-1909 (1965).

[35] J. Hölsa, M. Leskelä, and L. Niinistf, *Thermochim. Acta.*, **35**, 79-83 (1980).

[36] Y.D. Eagleman, E. Bournet-Courchesne, and S.E. Derenzo, *J. Lumin.*, **131**, 669-675 (2011).

[37] N. Imanaka and Y. Kato, *Chem. Commun.*, 1270-1271 (2003).

[38] N. Imanaka, N. Nunotani, K. Araki, and M. Yamane, *J. Am. Ceram. Soc.*, **101**, 1025-1028 (2018).

[39] Y. Kobayashi, T. Egawa, S. Tamura, and N. Imanaka, G. Adachi, *Chem. Mater.*, **9**, 1649-1654 (1997).

[40] A.L. Allred, *J. Inorg. Nucl. Chem.*, **17**, 215-221 (1961).

[41] J. Rodriguez-Carvajal, *Physica B*, **192**, 55-69 (1992).

[42] K. Momma and F. Izumi, *J. Appl. Crystallogr.*, **41**, 653-658 (2008).

[43] M.S. Islam, *J. Phys. Chem. Solids*, **51**, 367-372 (1190).

[44] W. Che, M. Wei, Z. Sang, Y. Ou, Y. Liu, and J. Liu, *J. Alloy. Compd.*, **731**, 381-388 (2018).

List of Publications

1. Novel Br^- Ion Conducting Solid Electrolyte Based on LaOBr

   Muhammad Radzi Iqbal Bin Misran, Naoyoshi Nunotani, Shinji Tamura, and Nobuhito Imanaka

   Journal of the Ceramic Society of Japan, **2018**, *126 (10)*, 761-765.

2. Enhancement of Bromide Ion Conductivity in Lanthanum Oxybromide Based Solids by Doping Divalent Zinc Ion with High Electronegativity

   Muhammad Radzi Iqbal Bin Misran, Naoyoshi Nunotani, Shinji Tamura, and Nobuhito Imanaka

   Journal of Asian Ceramic Societies, **2020**, *8 (3)*, 925-929.

3. Improvement of Bromide Ion Conduction in a Lanthanum Oxybromide Based Solid by Adjusting the Electronegativity of the Cation Dopant

   Muhammad Radzi Iqbal Bin Misran, Shinji Tamura, Naoyoshi Nunotani, and Nobuhito Imanaka

   Materials Letters, **2021**, *286*, 129211:1-4.

List of Supplementary Publications

1. Structural Environment of Chloride Ion-Conducting Solids Based on Lanthanum Oxychloride

   Naoyoshi Nunotani, **Muhammad Radzi Iqbal Bin Misran**, Miki Inada, Tomoki Uchiyama, Yoshiharu Uchimoto, and Nobuhito Imanaka

   Journal of the American Ceramic Society, **2020**, *103 (1)*, 297–303.

Acknowledgments

The author would like to extend his deepest appreciation to Professor Dr. Nobuhito Imanaka, Department of Applied Chemistry, Graduate School of Engineering, Osaka University, for his endless guidance, valuable opinions, and support during the course of this work.

The author heartfelt gratitude also goes to Dr. Shinji Tamura, Department of Applied Chemistry, Graduate School of Engineering, Osaka University, for his inspiring advice and discussions for conducting this work. The author is also obligated to Dr. Naoyoshi Nunotani, Department of Applied Chemistry, Graduate School of Engineering, Osaka University, for his guidance and constructive suggestions.

The author would like to express his sincere gratitude to Professor Dr. Akinori Saeki, Department of Applied Chemistry, Graduate School of Engineering, Osaka University, and Professor Dr. Masaya Nogi, Institute of Scientific and Industrial Research (Department of Applied Chemistry, Graduate School of Engineering), Osaka University, for their constructive and valuable comments during the revision of this thesis.

The author also sends his appreciation to the Government of Malaysia and the Iwatani Naoji Foundation for their financial support during the author's study.

The author also convey his gratitude to Dr. Hirokazu Izumi (Hyogo Prefectural Institute of Technology) for his help with the XPS measurements.

Words of gratitude also should be given to author's group partners, Dr. Bae Byungseo, Dr. Lee Wonrak, Dr. Abdul Rohman Supandi, Yusuke Kikkawa, Masanari Umeda, Yuji Hironaka, Shota Yamauchi, Lee Won Joon, Hiroaki Shirai, Kenji Matsuo, Mizuki Momai, Marina Taira, Takuya Kawaguchi, Kentaro Yamada, Koki Yoshikawa, Takato Ishimura, Wataru Ochi, Namiko Kato, Masaya Asahi for their continuous support and assistance during this work, and also the other members of Professor Dr. Nobuhito Imanaka's research group.

Finally, the author would like to express his deep gratitude to his parents, Mr. Misran Bin Rostam and Ms. Roziah Binti Ali, his brothers, Aiman Farhan Bin Misran, Armin Irfan Bin Misran, Muhammad Mikael Bin Misran, and to his dearest sister Fatin Nadhirah Binti Misran, her husband, Ashraf Bin Mohammad and their lovely new-born daughter, Aleesa Amanda Binti Ashraf, for their moral support, understanding and encouragement. Not to forget, to his uncle and aunt, Mr. Mohd. Noor Bin Ali and Ms. Marziana Binti Ab. Malib (Senior Lecturer, MARA University of Technology, Malaysia) and their family, for their continuous encouragement and advice.